Article

# Identification and Optimization of Mechanism-Based Fluoroallylamine Inhibitors of Lysyl Oxidase-Like 2/3.

Alison Findlay, Jonathan S. Foot, Alberto Buson, Mandar Deodhar, Andrew Jarnicki, Philip Hansbro, Gang Liu, Heidi Schilter, Craig Turner, Wenbin Zhou, and Wolfgang Jarolimek

*J. Med. Chem.*, **Just Accepted Manuscript** • DOI: 10.1021/acs.jmedchem.9b01283 • Publication Date (Web): 03 Oct 2019

# Identification and Optimization of Mechanism-Based Fluoroallylamine Inhibitors of Lysyl Oxidase-Like 2/3.

Alison D. Findlay,[†*] Jonathan S. Foot,[†*] Alberto Buson,[†] Mandar Deodhar,[†] Andrew G. Jarnicki,[‡⊥] Philip M. Hansbro,[‡#^] Gang Liu,[#^] Heidi Schilter,[†] Craig I. Turner,[†] Wenbin Zhou[†] and Wolfgang Jarolimek[†]

[†] Pharmaxis Ltd, 20 Rodborough Road, Frenchs Forest, Sydney, NSW 2086, Australia

[‡] Centre for Healthy Lungs, The University of Newcastle and Hunter Medical Research Institute, Newcastle, NSW 2300, Australia

[#] Centre for Inflammation, Centenary Institute, Sydney, NSW 2050, Australia

[^] University of Technology Sydney, Faculty of Science, Ultimo, NSW 2007, Australia

KEYWORDS Copper-dependent amine oxidase, lysyl oxidase, lysyl oxidase-like 2, lysyl oxidase-like 3, mechanism based enzyme inhibitors, collagen, elastin, fibrosis.

## ABSTRACT

Lysyl oxidase-like 2 (LOXL2) is a secreted enzyme that catalyzes the formation of cross-links in extracellular matrix proteins, namely collagen and elastin, and is indicated in fibrotic diseases. Herein we report the identification and subsequent optimization of a series of indole-based fluoroallylamine inhibitors of LOXL2. The result of this medicinal chemistry campaign is **PXS-5120A** (**12k**), a potent, irreversible inhibitor that is >300-fold selective for LOXL2 over LOX. **PXS-5120A** also shows potent inhibition of LOXL3, an emerging therapeutic target for lung fibrosis. Key to the development of this compound was the utilization of a compound oxidation assay. **PXS-5120A** was optimized to show negligible substrate activity *in vitro* for related amine oxidase family members, leading to metabolic stability. **PXS-5120A**, in a pro-drug form (**PXS-5129A**, **12o**), displayed anti-fibrotic activity in models of liver and lung fibrosis, thus confirming LOXL2 as an important target in diseases where collagen cross-linking is implicated.


## INTRODUCTION

In most organisms, including humans, two families of amine oxidases are responsible for the metabolism of various mono-, di- and polyamines produced endogenously or absorbed from exogenous sources. The first of these families use covalently bound flavin adenine dinucleotide (FAD) as the cofactor, and includes the monoamine oxidases (MAOs; MAO-A and MAO-B), involved in the metabolism of neuroactive amines such as dopamine, serotonin and norepinephrine;[1] polyamine oxidase (PAO), which oxidatively deaminates spermine and

spermidine;[2] and lysine-specific histone demethylases, such as LSD1 (or KDM1A), that are involved in epigenetic function.[3]

The second family of amines oxidases are dependent on copper and utilize an oxidized tyrosine residue as the cofactor.[4] Within this family there are two sub-classes. The first one consists of the Amine Oxidase, Copper-containing (*AOC*, utilizing the topaquinone (TPQ) cofactor) sub-class encompassing diamine oxidase (DAO; *AOC1*), involved in the metabolism of histamine;[5] retinal specific amine oxidase (RAO; *AOC2*) found predominantly in the eye;[6] semicarbazide-sensitive amine oxidase (SSAO, also known as vascular adhesion protein-1 (VAP-1); *AOC3*), an ectoenzyme involved in leukocyte recruitment;[7] and plasma amine oxidase (*AOC4*) which is found in all mammals except rats, mice and humans (who lack a functional *AOC4* gene).[8] The second sub-class consists of the lysyl oxidase family (utilizing the lysine tyrosylquinone (LTQ) cofactor).

There are 5 members of the human lysyl oxidase protein family, designated lysyl oxidase (LOX) and lysyl oxidase-like 1-4 (LOXL1-4).[9] The expression pattern of LOX family members can alter depending on cell type, differentiation state, development state and disease state.[10] The LOX family act as key regulators in the cross-linking of elastin and collagen fibrils, through the oxidation and condensation of the ε-amino group of specific lysine and hydroxylysine residues.[11] A fine balance of elasticity and mechanical stiffness is required to maintain appropriate function in various tissues such as the lung and heart, and this balance is dependent on LOX/LOXL activity.[12] Up-regulation of one or more of the LOX family enzymes can lead to aberrant cross-linking, causing excessive local collagen deposition and propagation of pro-fibrotic signaling within the extracellular matrix (ECM). If left unchecked, this can induce tissue scarring, fibrosis and destruction of function, eventually leading to organ failure.[13]

Under normal physiological conditions, LOX is ubiquitously expressed in most human tissues at higher levels than other family members,[10] and is essential in the development of healthy bone, respiratory system and cardiovascular function.[14,15,16] In contrast, LOXL2 mRNA and protein levels are upregulated in fibrotic tissues and diverse solid tumors when compared with normal human tissues.[17] LOXL2 is also considered a biomarker for progression in various diseases, such as liver and lung fibrosis, scleroderma and cancer.[18,19,20,21] Given the important role that LOXL2 appears to play in certain fibrotic diseases, selective inhibition of LOXL2 over LOX offers clear advantages for their long-term treatment.

LOXL2 is significantly increased in human cholangiopathies, and is proposed to contribute to bile duct injury through suppression of E-cadherin in biliary epithelial cells.[22] Ikenaga *et al.* have shown that LOXL2 mediates collagen crosslinking and fibrotic matrix stabilization during liver fibrosis, and independently promotes fibrogenic hepatic progenitor cell (HPC) differentiation.[23] Moreover, using the murine LOXL2 antibody AB0023,[24] the authors have shown that inhibition of LOXL2 can promote a reversal of advanced parenchymal liver fibrosis in mice. How critical the role of LOXL2 and its enzymatic activity is in hepatic fibrosis compared to the other members of the LOX family is yet to be fully proven,[25] with evidence that in some instances LOX can also act as biomarker for liver fibrosis.[26]

LOXL2 is also of interest as a therapeutic target in lung fibrosis, including idiopathic pulmonary fibrosis (IPF).[27] LOXL2 is over-expressed in patients with IPF[28] and is reported to activate lung fibroblasts via regulation of the TGF‑β/Smad signaling pathway.[29]

A humanized monoclonal LOXL2 antibody AB0024 (Simtuzumab) had been advanced into clinical trials, including two fibrosis indications (IPF and NASH).[30,31] Whilst Simtuzumab was

found to be safe and well tolerated, there was no sign of clinical benefit. Although this result has thrown doubt on the viability of LOXL2 as a target, it is important to note that the antibody only partially (~40%) inhibits the catalytic activity of the enzyme,[17a,24] and is therefore unlikely to have a significant effect on collagen cross-linking. Additionally, the absence of a pharmacodynamic assay for LOXL2 inhibition meant that confirmation of target inhibition with these dosing regimens was not confirmed, nor was penetration into the organ of interest.[30] To this end, a small molecule with appropriate drug-like qualities offers an opportunity to fully evaluate the therapeutic potential of LOXL2 inhibition.

Scarce examples of small molecule lysyl oxidase inhibitors exist, with *β*-aminopropionitrile (BAPN) (Figure 1) long serving as the archetypal pan-LOX inhibitor.[32] More recently, Springer *et. al.*[33] disclosed an aminomethylthiophene-based inhibitor CCT365626 (**1**) with sub-micromolar potency for both the LOX and LOXL2 isoforms, however no selectivity data was provided for the other family members. PharmAkea have reported the development of a series of aminomethyl pyridine-based, selective LOXL2 inhibitors,[34] of which PAT-1251 (**2**) completed Phase I trials at the end of 2016.[35] Although enzyme inhibition in humans seems to have been achieved with **2**, it appears short lived (complete recovery 24 h after a single dose of 1000 mg per healthy volunteer was reported),[36] and the therapeutic implications of such a profile are at present unclear.

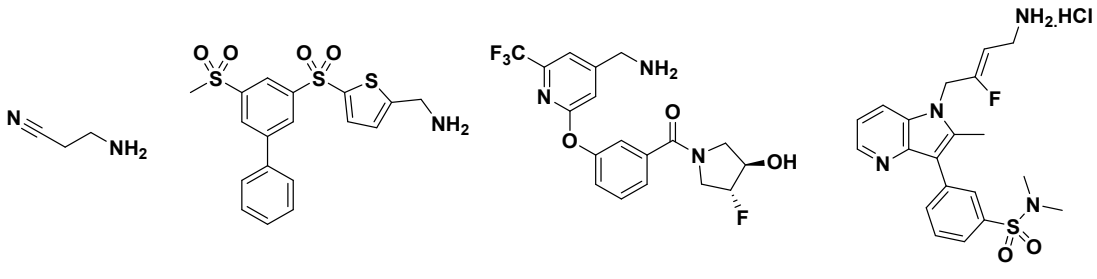


**Figure 1.** Chemical structures of BAPN, CCT365623 (**1**), PAT-1251 (**2**) and PXS-5153A (**3**)

We have recently reported the structure of **PXS-5153A (3)**, and outlined its efficacy in two models of liver fibrosis and a model of myocardial infarction.[17b] **PXS-5153A** was developed in tandem to the chemical series reported herein with the purpose of producing a tool compound to establish proof-of-concept for *in vivo* inhibition of LOXL2 in models of fibrosis. **PXS-5153A** was found to have good potency for LOXL2 ($pIC_{50}$ = 7.7, see also Table 3) and reasonable selectivity over LOX (~70-fold, see also Table 3). Importantly **PXS-5153A** was found to possess a pharmacokinetic profile that allowed for low dosing of the molecule in *in vivo* models. Unfortunately **PXS-5153A** is recognized as a substrate by both SSAO and plasma amine oxidase (data shown in Table 3), and that precluded the molecule from being developed further. The present work outlines the identification and optimization of an indole-based structural class (closely related to **PXS-5153A**) and strategies to improve on the potency, selectivity and, most importantly, potential for oxidation by SSAO and plasma amine oxidase, the latter to enable pre-clinical toxicological evaluation of this class of LOXL2 inhibitors in higher order mammals (dog, pig, monkey, etc.).

These studies led to the identification of **12k** (**PXS-5120A**), a potent LOXL2/3 inhibitor which demonstrated efficacy in models of both liver and lung fibrosis, in addition to the previously reported benefits in a diabetic nephropathy model.[37]

## INHIBITOR DESIGN

Common to the quinone-containing AOC family of enzymes is the ability to recognize and oxidize short length arylalkyl-based primary amines (histamine, dopamine, tyramine, benzylamine). With SSAO/VAP-1, this has been exploited using a variety of 3, 4 and 5-atom length arylsubstituted fluoroallylamine groups (e.g. mofegiline, PXS-4159A, LJP 1586, PXS-4681A)[38-41] These fluoroallylamines are recognized as substrates and are therefore capable of binding to the quinone

cofactor directly. In the case of SSAO, it is thought that this leads to the activation of the previously unreactive vinyl fluoride moiety towards nucleophilic attack, thereby enabling formation of a further covalent bond within the active site and irreversibly inhibiting enzyme function (Scheme 1).[42]

**Scheme 1.** Proposed mechanism of inhibition of SSAO/VAP-1 by fluoroallylamine-based compounds[a]

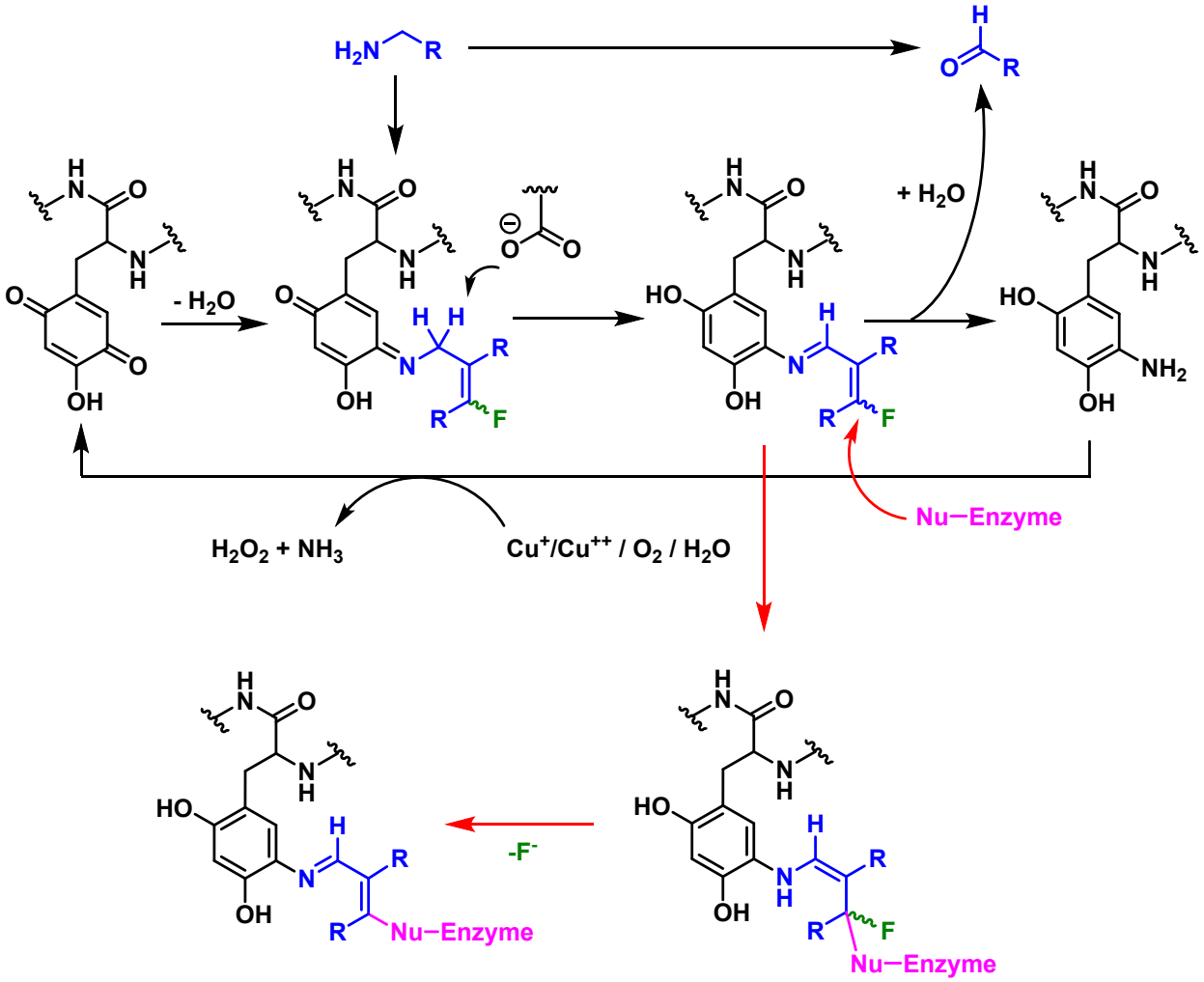


[a] Scheme shows the proposed mechanism of inhibition of SSAO by fluoroallylamine-based inhibitors. Black arrows portray the normal catalytic turnover of amine substrates, the red arrows show how the installation of a vinyl fluoride

into the molecule can redirect the pathway, resulting in the covalent alkylation of the protein active site. "Nu": nucleophilic amino acid residue in the active site.

Given the success of this approach in selectively targeting the SSAO TPQ cofactor, we sought to design a novel series of inhibitors of LOXL2 based on a similar tactic, targeting the LTQ cofactor. As no detailed structural information regarding the target was available at the outset of our synthetic campaign[43] we screened several fluoroallylamine templates to identify a tractable starting point and extend the utility of these scaffolds. We found that a previously reported fluoroallylamine **4**,[44] displayed modest LOXL2 inhibition, albeit with no selectivity over LOX (Figure 2) nor SSAO. Further exploration of the fluoroallylamine motif afforded the (*Z*)-isomer, **5**, a compound with improved LOXL2 potency and reduced SSAO activity. This fluoroallylamine configuration was deemed to be a suitable starting point for further investigation.

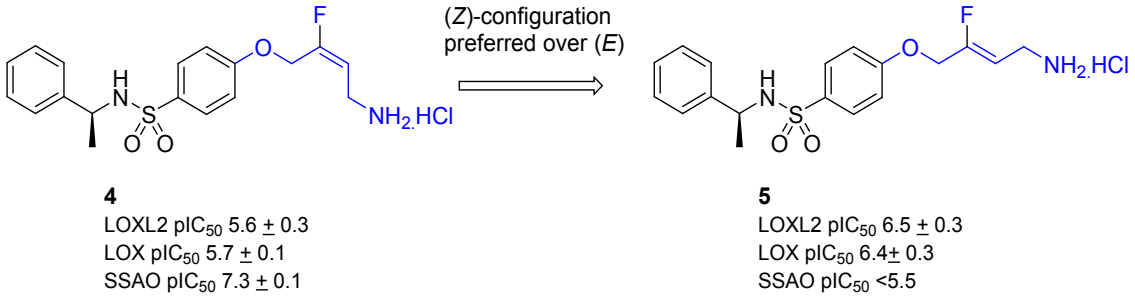


**4**
LOXL2 $pIC_{50}$ 5.6 ± 0.3
LOX $pIC_{50}$ 5.7 ± 0.1
SSAO $pIC_{50}$ 7.3 ± 0.1

**5**
LOXL2 $pIC_{50}$ 6.5 ± 0.3
LOX $pIC_{50}$ 6.4± 0.3
SSAO $pIC_{50}$ <5.5

**Figure 2.** Identification of a suitable fluoroallylamine configuration.

## RESULTS AND DISCUSSION

With a view to identifying the features necessary for boosting LOXL2 potency and opening a selectivity window over LOX, we opted to replace the central linking phenol moiety appended to the fluoroallylamine in **5** with a 1,2,3-triazole and expand on the substitution of the terminal phenyl ring. This enabled rapid exploration *via* Cu(I)-catalyzed Huisgen cycloaddition reaction[45] between

appropriately functionalized alkynes **6a-h** and azide **9**, derived from the previously reported alcohol **7**,[44] affording a suite of 1,2,3-triazole-based inhibitors **10a-h** (Scheme 2 and Table 1). While recombinant human LOXL2 was used for functional assays, bovine aorta LOX was utilized for selectivity screening the analogues, as it was found that this was pharmacologically similar to human fibroblast LOX and was more readily available.

**Scheme 2.** Synthesis of 1,2,3-triazole-based inhibitors **10a-h**

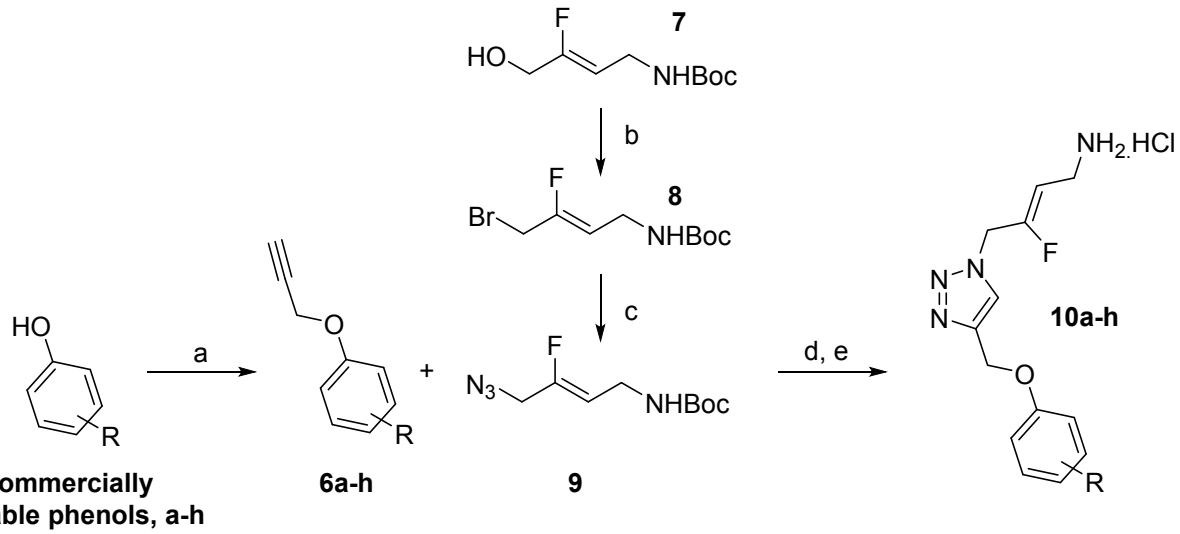


Reagents and conditions: (a) propargyl bromide, $K_2CO_3$, MeCN, rt; (b) MsCl, $Et_3N$, acetone, then LiBr, 0 °C-rt; (c) $NaN_3$, DMF, rt; (d) $CuSO_4(H_2O)_5$, sodium ascorbate, *t*-BuOH, rt; (e) (i) TFA, DCM, rt; (ii) HCl, $Et_2O$ / EtOAc, rt.

**Table 1.** LOXL2 and LOX inhibition by 1,2,3 triazole analogues **10a-h**

| Compound | R group | LOXL2[a,b,c] ($pIC_{50}$ ± SD) | LOX[a,b,c] ($pIC_{50}$ ± SD) |
|---|---|---|---|
| **BAPN** | n/a | 6.4 ± 0.12 | 5.7 ± 0.13 |
| **10a** | H | 6.5 ± 0.08 | 6.3 ± 0.2 |
| **10b** | 4-*t*Bu | 6.1 ± 0.05 | 6.3 ± 0.2 |
| **10c** | 4-$SO_2$Me | 6.7 ± 0.3 | 6.2 ± 0.1 |

| | | | |
|---|---|---|---|
| **10d** | 2-$SO_2Me$ | 5.7 ± 0.07 | 5.5 ± 0.2 |
| **10e** | 3-$SO_2Me$ | 6.1 ± 0.05 | 6.0 ± 0.05 |
| **10f** | 4-$CONMe_2$ | 6.1 ± 0.1 | 5.5 ± 0.4 |
| **10g** | 4-$SO_2NMe_2$ | 7.3 ± 0.1 | 6.1 ± 0.2 |
| **10h** | 2-Cl, 4-$SO_2NMe_2$ | 7.7 ± 0.09 | 6.1 ± 0.2 |

[a] The measurement of enzymatic activities was based on the detection of hydrogen peroxide with an Amplex-Red oxidation assay[46]; [b] Minimum of n=2 for each experiment; [c] "LOXL2" = recombinant human LOXL2 and "LOX" = bovine aorta LOX; SD = standard deviation

Introduction of simple alkyl groups such as a *t*-butyl group (**10b**) was found to have a slightly detrimental effect on LOXL2 potency relative to the unsubstituted example, **10a**, while introduction of the electron withdrawing methyl sulfone marginally improved potency (**10c**), importantly favoring LOXL2 over LOX (Table 1). In terms of the optimal position for substitution, 4-$SO_2Me$ was preferred over 2-$SO_2Me$ (**10d**) and 3-$SO_2Me$ (**10e**). While replacement of the para-methyl sulfone with 4-$CONMe_2$ (**10f**) showed no benefit, a significant improvement in LOXL2 potency was achieved upon introduction of the dimethylsulfonamide moiety, as in **10g**. The introduction of a chloro substituent in the *ortho*-position in **10h** resulted in a further increase in LOXL2 potency. Evaluation of **10g** and **10h** for off-target amine oxidase activity showed that although neither inhibited SSAO ($pIC_{50}$ <4.5) both were inhibitors of DAO ($pIC_{50}$ of 6.5 for each), and **10g** (but not **10h**) also inhibited MAO-B ($pIC_{50}$ 6.9).

Given the presence of the primary amine, we next evaluated the most potent analogues to establish if these compounds were recognized as substrates.

Amine oxidase substrate activity may effectively act as a clearance pathway, reducing available inhibitor levels. Furthermore, it has the potential to produce oxidative stress and undesirable species *in vivo*, owing to the fact that hydrogen peroxide and the corresponding aldehyde species are by-products of the enzyme reaction. In addition, plasma amine oxidase substrate activity can complicate pre-clinical development, due to its differential presence between species (aside from rodents and humans, the *AOC4* gene product is present in all mammalian species, especially the dog).[8] Thus, rapid "turnover" by the related amine oxidases was potentially a major limitation and recognized as an important development consideration. To monitor, and thereby enable optimization of this, compound oxidation assays to measure the relative substrate activity by SSAO and plasma amine oxidase were introduced into the screening cascade.

Both compounds were rapidly turned over in the SSAO and plasma amine oxidase oxidation assays, and when incubated in dog plasma, **10h** was found to be completely consumed, with 0% parent compound remaining after 1 hour. Pre-incubation of the dog plasma with semicarbazide (to inhibit SSAO and plasma amine oxidase) confirmed that this degradation was dependent on the activity of these related amine oxidases (data not shown).

In efforts to improve these aspects, we opted to explore the effect of both linker and core modifications (Figure 3). Due to the observed high turnover by SSAO of the triazole-linked compounds, we chose to first evaluate this parameter and identify an alternative chemo-type that would not be recognized as a substrate by SSAO.

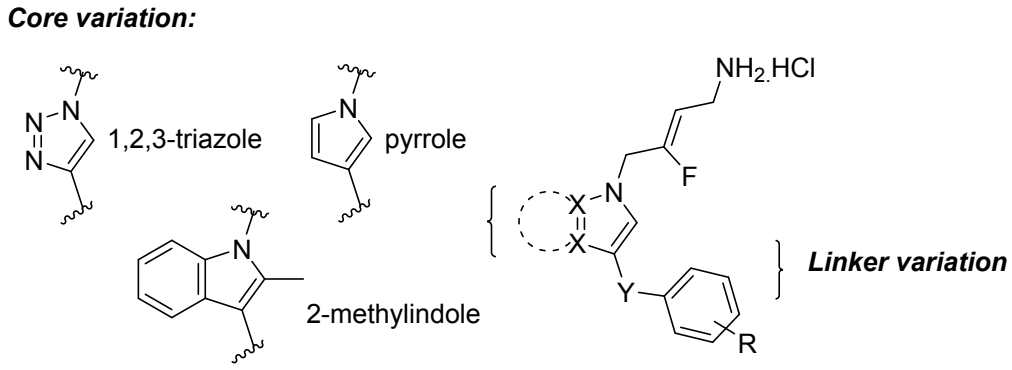


**Figure 3.** Variation of linker and core regions.

**Table 2.** Structure-activity relationships of linker and core-based modifications

| Compound | Linker, Y | Core | 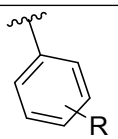 | LOXL2[a,b] ($pIC_{50}$ ± SD) | LOX [a,b] ($pIC_{50}$ ± SD) | oxidation by SSAO[c] |
|---|---|---|---|---|---|---|
| **10g** | $CH_2O$ | 1,2,3-triazole | 4-$SO_2NMe_2$ | 7.3 ± 0.1 | 6.1 ± 0.2 | >4 |
| **10i** | $CH_2NH$ | 1,2,3-triazole | 4-$SO_2NMe_2$ | 7.7 ± 0.02 | 6.3 ± 0.2 | >4 |
| **10j** | $CH_2$ | 1,2,3-triazole | 4-$SO_2NMe_2$ | 7.9 ± 0.01 | 6.2 ± 0.2 | >4 |
| **10k** | - | 1,2,3-triazole | 4-$SO_2NMe_2$ | 6.9 ± 0.3 | 6.1 ± 0.09 | >4 |
| **11a** | - | pyrrole | 4-$SO_2NMe_2$ | 6.6 ± 0.04 | 6.1 ± 0.1 | >4 |
| **11b** | - | pyrrole | 3-$SO_2NMe_2$ | 7.0 ± 0.04 | 5.7 ± 0.2 | >4 |
| **12a** | - | 2-Me indole | 4-$SO_2NMe_2$ | 6.1 ± 0.04 | 5.5 ± 0.1 | 2.8 |
| **12b** | - | 2-Me indole | 3-$SO_2NMe_2$ | 7.0 ± 0.07 | 5.7 ± 0.1 | 1.4 |

[a] The measurement of enzymatic activities was based on the detection of hydrogen peroxide with an Amplex-Red oxidation assay[46]; [b] Minimum of n=2 for each experiment; [c] Compound oxidation assay measuring the amount of hydrogen peroxide generated at a single concentration (30 μM) of compound, relative to DMSO; SD = standard deviation

Alternative linkers ($CH_2NH$, **10i**, and $CH_2$, **10j**, in place of $CH_2O$) revealed little difference in terms of potency relative to **10g** (Table 2), nor in turnover by SSAO. Removing rotatable bonds to the biaryl structure **10k** was tolerated, providing a more compact and less flexible structure with reasonable potency for LOXL2 and good selectivity over LOX, however significant SSAO turnover was still observed. Replacing the 1,2,3-triazole with a pyrrole (**11a** and 1**1b)** maintained potency without improving turnover. Moving to the 2-methylindole scaffold with a direct link to the aryl sulfonamide (**12a** and **12b**) resulted in a reduction in turnover by SSAO. Presumably this improvement was due to the increase in steric bulk attached directly to the fluoroallylamine warhead rather than an electronic effect, given the turnover of the related pyrroles **11a** and **11b**. Interestingly for both the pyrroles and indoles, a switch from *para*- to *meta*-$SO_2NMe_2$ provided an increase in LOXL2 potency as well as improved selectivity over LOX.

Further profiling against the family of amine oxidases showed **12b** to be a highly selective inhibitor of LOXL2, with no inhibition of MAO-A or B ($pIC_{50}$s <4.5), and minimal activity towards SSAO or DAO ($pIC_{50}$ of 5.1 and 5.4 respectively). However, despite these improvements, **12b** was rapidly turned over by plasma amine oxidase, meaning that further modification was required to enable identification of a compound suitable for preclinical evaluation in higher mammals (*e.g.* dog, monkey, pig). Equally, additional improvements in selectivity were desired to enable accurate evaluation of the effects of LOXL2 inhibition over LOX in preclinical models of disease.

As the 3-substituted dimethylsulfonamide aryl ring appeared necessary for LOXL2 potency and selectivity over LOX, we chose to "fix" this moiety and investigate substitution of the indole aromatic ring (Scheme 3 and Table 3). Introduction of an electron-withdrawing dimethyl amide group (**12c**, **12d** and **12e**) at the 5, 6 or 7-position significantly improved SSAO and plasma amine oxidase substrate activity such that these compounds were not turned over at all by either enzyme.

Potency for the 5- and 6-substituted examples also significantly improved, however the 7-substituted example showed a dramatic drop-off in LOXL2 inhibition. Given the slightly better potency displayed by **12c**, further examples were pursued with substitution in the 5-position. A chloro group was equally well tolerated (**12f**), as was a free phenol group (**12g**), however switching to the methoxy group (**12h**) drastically increased turnover by SSAO. A reverse sulfonamide (**12i**) also showed an increase in plasma amine oxidase turnover. Introduction of a methyl sulfone (**12j**) improved LOXL2 potency further, but this was accompanied by an increase in turnover by SSAO and plasma amine oxidase. Switching to a carboxylic acid afforded a similarly potent compound **12k** (**PXS-5120A**) with improved selectivity over LOX (>300-fold) and minimal turnover, an effect that was not mirrored in the 6-position (**12l**). Tetrazole (**12m**) was not a viable bioisosteric replacement of the carboxylic acid in this case, leading to a drop in potency, whilst the ethyl ester **12o** (**PXS-5129A**), which can be regarded as a pro-drug form of **12k** (**PXS-5120A**), had good potency but moderate SSAO turnover. Removal of the fluorine group from the allylamine warhead (**12n**, also Figure 4D) led to a 100-fold drop in potency, consistent with its proposed role in the mechanism of inhibition.

**Scheme 3.** Synthesis of 2-methyl, 3-aryl indole-based inhibitors **12b-12o**[a]

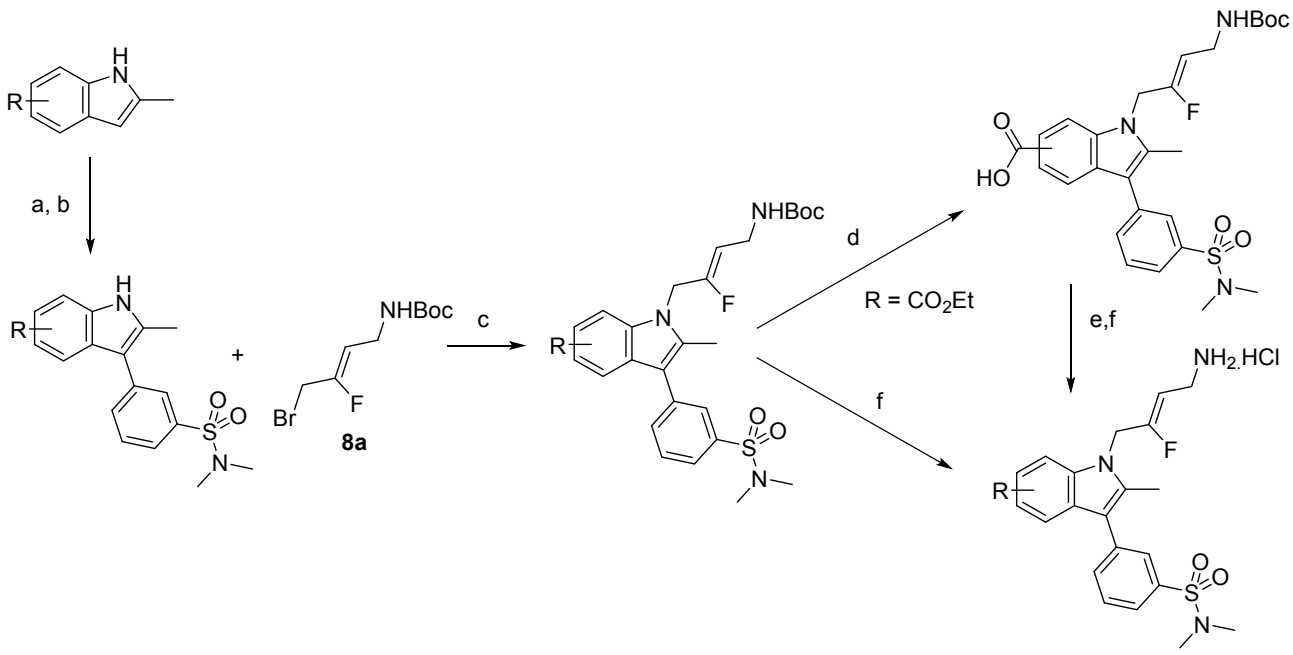


[a] Reagents and conditions: (a) NBS, then DMAP, $Boc_2O$, $CH_2Cl_2$, rt; (b) aryl boronic acid/ester, $Pd(PPh_3)_4$, $K_2CO_3$ (aq), dioxane, 80 °C, then TFA, $CH_2Cl_2$, rt; (c) $Cs_2CO_3$, DMF, rt; (d) LiOH, MeOH, THF, $H_2O$, rt; (e) if R = $CONMe_2$ group, then $Me_2NH$, HATU, DIPEA, DMF, rt; (f) Either 2 M HCl (in $Et_2O$), MeOH, or TFA, $CH_2Cl_2$, then HCl (in $Et_2O$).

**Table 3.** Optimization of the indole core

| Compound | R group | LOXL2 [a,b] ($pIC_{50}$ ± SD) | LOX [a,b] ($pIC_{50}$ ± SD) | Oxidation by SSAO[c] | Oxidation by *AOC4*[c] |
|---|---|---|---|---|---|
| **12b** | H | 7.0 ± 0.07 | 5.7 ± 0.1 | 1.4 | >4 |
| **12c** | 5-$CO_2NMe_2$ | 7.6 ± 0.14 | 5.8 ± 0.20 | 1.2 | 1 |
| **12d** | 6-$CO_2NMe_2$ | 7.2 ± 0.02 | 6.1 ± 0.01 | 1 | 1.1 |
| **12e** | 7-$CO_2NMe_2$ | 5.5 ± 0.05 | 4.7 ± 0.11 | 1.1 | 1.4 |
| **12f** | 5-Cl | 6.9 ± 0.11 | 5.5 ± 0.03 | 1.2 | 1.1 |
| **12g** | 5-OH | 7.3 ± 0.03 | 5.9 ± 0.18 | 1 | 1.1 |

| | | | | | |
|---|---|---|---|---|---|
| **12h** | 5-OMe | 7.1 ± 0.10 | 5.8 ± 0.04 | 4.6 | 1.6 |
| **12i** | 5-$NHSO_2Me$ | 7.7 ± 0.07 | 6.0 ± 0.07 | 1 | 1.5 |
| **12j** | 5-$SO_2Me$ | 8.3 ± 0.17 | 6.4 ± 0.06 | 1.3 | 1.3 |
| **12k PXS-5120A** | 5-$CO_2H$ | 8.4 ± 0.04 | 5.8 ± 0.10 | 1 | 1 |
| **12l** | 6-$CO_2H$ | 6.3 ± 0.02 | 4.8 ± 0.03 | 1.1 | 1 |
| **12m** | 5-tetrazole | 6.9 ± 0.03 | 4.8 ± 0.21 | -[d] | 1 |
| **12n** | 5-$CO_2H$ *des*-Fluoro | 6.1 ± 0.07 | 5.5 ± 0.18 | 1 | 1.3 |
| **12o PXS-5129A** | 5-$CO_2Et$ | 7.1 ± 0.09 | 5.2 ± 0.12 | 2.4 | 1 |
| **PXS-5153A** | n/a | 7.7 ± 0.23 | 5.9 ± 0.09 | 1.6 | 6.4 |

[a] The measurement of enzymatic activities was based on the detection of hydrogen peroxide with an Amplex-Red oxidation assay[46]; [b] Minimum of n=2 for each experiment; [c] Compound oxidation assay measuring the amount of hydrogen peroxide generated at a single concentration (30 μM) of compound, relative to DMSO; [d] Not tested; SD = standard deviation

**PXS-5120A** (**12k**) exhibited good selectivity over the related amine oxidase enzymes and showed limited auxiliary pharmacology in standard profiling assays (the compound was tested at 10 μM against 119 different off-targets; see Supporting Information. Only the peripheral benzodiazepine receptor was inhibited by >50%). Importantly, **PXS-5120A** exhibited similar potency for LOXL2 across all species tested (Table 4), allowing for easier translation of our *in vivo* findings when transitioning into the clinic. In a functional assay measuring the ability of the compound to inhibit the crosslinking of rat collagen *in vitro*,[17b] **PXS-5120A** displayed dose-dependent inhibition of crosslinking, with a calculated $IC_{50}$ of 13 nM. Comparison with **PXS-5153A** in the same assay showed this to be a ~3-fold improvement, in line with the improved potency in the primary LOXL2 assay (see Supplementary Figure S1 and Table 3). **PXS-5120A** is metabolically stable *in vitro* and has moderate protein plasma binding.

**Table 4.** *In vitro* profile of **12k** (**PXS-5120A**)

| **Assay- potency and selectivity** | **$IC_{50}$ (nM)** |
|---|---|
| Recombinant human LOXL2 | 5 |
| Human fibroblast LOXL2 | 9 |
| Recombinant mouse LOXL2 | 6 |
| Recombinant rat LOXL2 | 6 |
| Collagen oxidation assay | 13 |
| Recombinant human DAO | >10000 |
| Recombinant human SSAO, MAO-A/B | >30000 |
| Human fibroblast LOX | 1260 |
| Bovine LOX (aorta) | 1780 |
| Murine LOX (lung fibroblasts) | 1754 |
| Recombinant human LOXL1 | 2260 |
| Recombinant human LOXL3 | 16 |
| Recombinant human LOXL4 | 280 |

| **Assay – ADME parameters** | **Result** |
|---|---|
| PPB (rat/dog/human), % bound | 88/86/92 |
| Plasma stability (rat, dog & human) $t_{1/2}$ | >120 mins |
| Microsomal stability (rat, dog & human) $t_{1/2}$ | >90 mins |
| Hepatocyte stability (rat, dog & human) $t_{1/2}$ | >120 mins |

Profiling of the other LOXL family members (Table 4) shows that **PXS-5120A** is a potent inhibitor of the LOXL3 enzyme, and a moderate blocker of LOXL4. The reason for selectivity for the LOXL2/3 enzymes over LOXL4 is not immediately obvious. All three of these LOXL enzymes are closely related in terms of protein domains, expressing a signal peptide domain and four scavenger receptor cysteine-rich (SRCR) domains, in addition to their catalytically active LOX domain (in contrast to the LOX and LOXL1 isoforms that are secreted in a propeptide form devoid of SRCR domains). All three possess a high degree of homology at the C-terminal enzymatically active region of the peptide.[10] Given the lack of structural information concerning the active forms of the LOX enzymes,[43] comparisons of the active sites are limited to analysis of residues in the immediate vicinity of the LTQ cofactors and the copper binding domains. One potentially significant difference between the LOXL2/3 isoforms and LOXL4 is observed between the four conserved histidine residues in the copper binding domain, wherein the presence of negatively charged aspartate (LOXL2) and glutamate (LOXL3) residues is in contrast to a neutral glutamine residue in LOXL4. It is possible that these negatively charged residues impart a subtle structural change, leading to the observed preference of **PXS-5120A** for LOXL2/3 over LOXL4.

Interestingly, LOXL3 has recently been implicated in the pathology of pulmonary fibrosis,[27] where it is thought to be involved in both the activation of fibroblasts, and the transition of fibroblasts to myofibroblasts. Upregulation of both LOXL2 and LOXL3 has also been observed in a carbon tetrachloride ($CCl_4$)-driven rat model of liver fibrosis, suggesting that both enzymes may play a role in the development of acute hepatic injury as well.[17b] These reports indicate that inhibition of LOXL2, with additional inhibition of LOXL3, would represent a more effective approach for disease modulation than targeting a single protein, and therefore have a higher chance in the successful treatment of fibrotic lung and liver disease.

**PXS-5120A** displayed a) time-dependent LOXL2 inhibition (apparent $K_i$ = 83 nM and $k_{inact}$ = 0.89 $min^{-1}$) (Figure 4A and Supplementary Figure S2); b) substrate competition, in which increasing concentrations of the reference substrate, putrescine, reduced inhibition by **PXS-5120A** in a competitive manner (Figure 4B) and c) irreversible inhibition in jump dilution experiments, in which, after 100-fold dilution from a 30 x $IC_{50}$ concentration of the inhibitor, maximal inhibition (>80%) of the enzyme activity was maintained when substrate was re-introduced (Figure 4C). To confirm that the mechanism of inactivation was indeed driven by the presence of the fluoroallylamine group on the warhead, the *des*-fluoro analogue **12n** was profiled head to head with **PXS-5120A** (Figure 4D) in a bound LOXL2 washout assay. Monitoring the enzyme activity for 30 minutes after washout showed that **12n** had been mostly displaced, whereas **PXS-5120A** (and BAPN) prevented recovery of enzyme activity, reaffirming that the vinyl fluoride plays a critical role in the mechanism of inhibition of the enzyme. Furthermore, analysis of compound oxidation (in the absence of substrate) of **12n** vs **PXS-5120A** by LOXL2, in a similar manner to what has been described above for SSAO and plasma amine oxidase, shows that whereas **PXS-5120A** has no detectable substrate activity (oxidative turnover after 30 min relative to DMSO = 1), **12n** is turned over substantially (relative oxidation = 6 at 30 mins). Taken together these observations support the hypothesis that **PXS-5120A** acts as an irreversible inhibitor of LOXL2 through a mechanism based on the displacement of the fluorine atom from the fluoroallylamine warhead moiety. Further experiments (e.g. protein digest – LCMS or X-ray crystallography) would be required to unequivocally prove the proposed mode of action of **PXS-5120A** and verify if it is covalently bound to the cofactor.

**Figure 4.** Mechanistic studies on **4** (**PXS-5120A**)

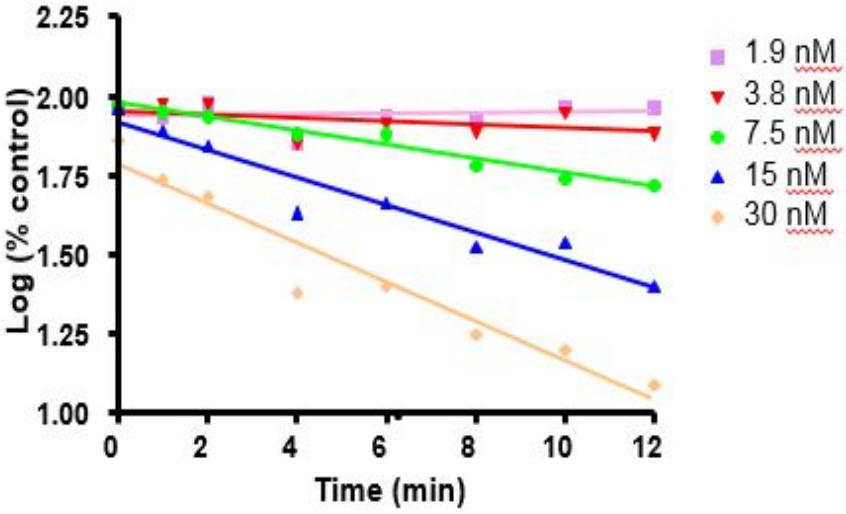


**(A)** LOXL2 inhibition by **PXS-5120A** is time dependent.

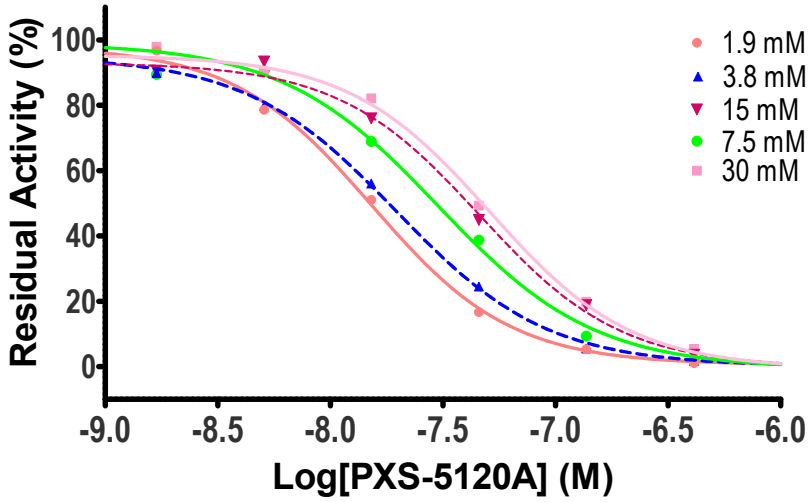


**(B)** Substrate competition; Rising concentrations of the substrate putrescine compete with LOXL2 inhibition by **PXS-5120A**, suggesting that **PXS-5120A** acts directly through interacting with the catalytic cofactor.

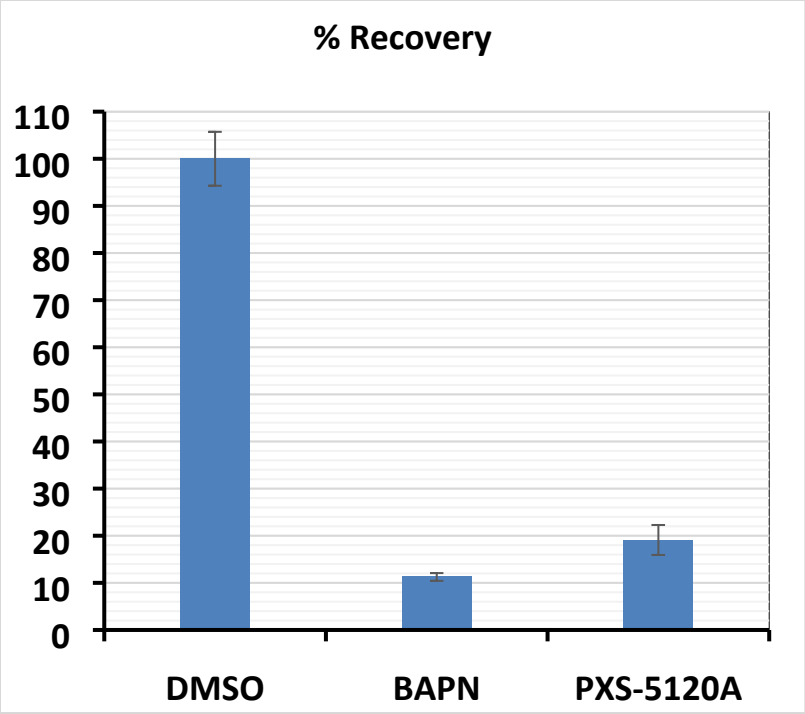


**(C)** Jump dilution; 1 h soak with inhibitor (at a concentration equivalent to 30 x $IC_{50}$) followed by a 100-fold dilution, before addition of putrescine. Assay readout at 30 minutes after substrate addition. No significant return of activity was observed for either BAPN or **PXS-5120A**.

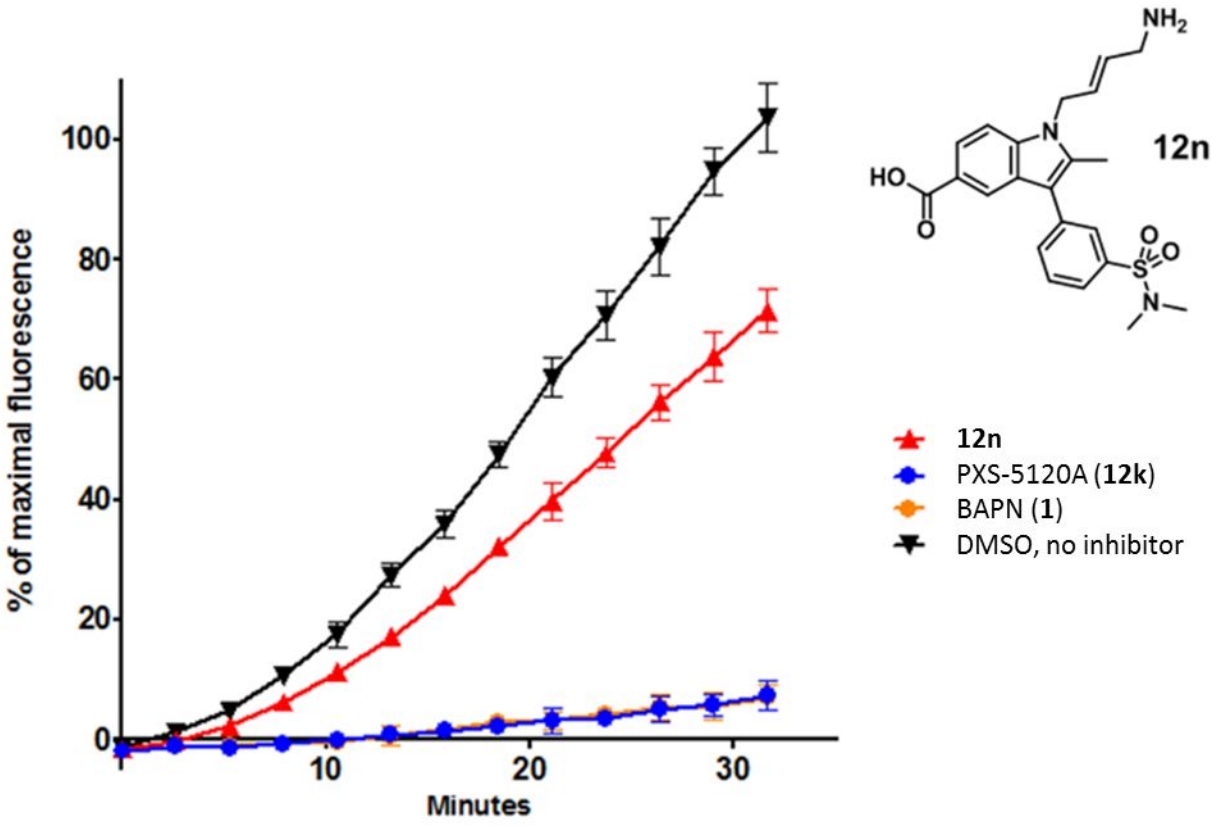


**(D)** Washout experiment using bound LOXL2; Time course of substrate turnover post washout showing the return of enzyme activity over time after exposure to the inhibitor. Neither **PXS-5120A** nor BAPN (plots overlapping) showed any return of activity over background after 30 mins. Des-fluoro **PXS-5120A**, **12n**, shows a return of enzyme activity to a level of ~75% of that observed where no inhibitor was present pre-washout.

**PXS-5120A** was found to be poorly absorbed and rapidly excreted in both rats and mice, leading to very low oral bioavailability (<1%, data not shown). **PXS-5129A**, however, was found to be readily absorbed following oral gavage, and once in the circulation, rapidly hydrolyzed to release **PXS-5120** (free base) *in vivo*, affording plasma concentrations well above the LOXL2 $IC_{50}$ (6 nM, equivalent to ~3 ng/mL) for a prolonged period (>6 hours) in mice, whilst remaining well below the $IC_{50}$ for LOX throughout (Figure 5).

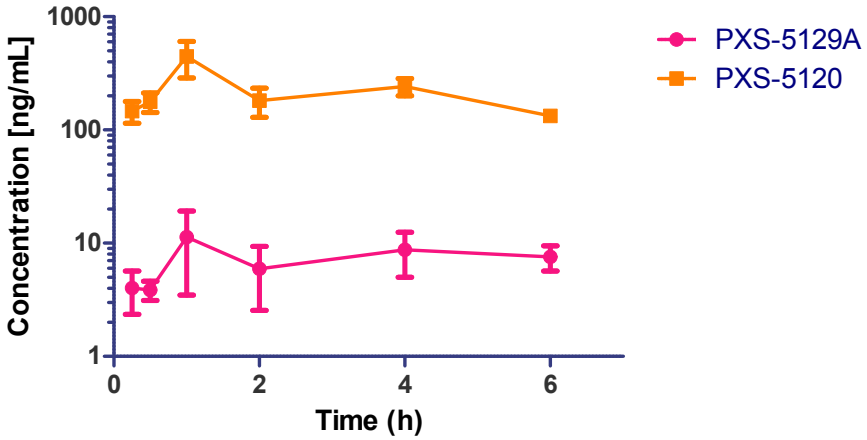


**Figure 5.** Mouse plasma profile of **PXS-5120** (free base of **PXS-5120A**) after oral (20 mg/kg) administration of the corresponding ethyl ester, **PXS-5129A**. Pharmacokinetic analysis of **PXS-5129A** and **PXS-5120** in BALB/c mice, showing the hydrolysis of **PXS-5129A** *in vivo* to afford therapeutically relevent plasma concentrations of **PXS-5120**. The plasma concentrations of both **PXS-5129A** and **PXS-5120** were quantified by LCMS/MS. Each data point represents an average of 3 animals.

With the drug/pro-drug pairing of **PXS-5120A/5129A** in hand we next sought to test the theory that selective inhibition of LOXL2 (and LOXL3) over LOX could affect a therapeutic outcome in relevant models of disease where LOXL2 was either significantly upregulated or has been shown to play a clear role in the disease pathology through aberrant collagen cross-linking.

To evaluate **PXS-5120A/PXS-5129A** as a potential therapy for hepatic injury, a 6-week carbon tetrachloride ($CCl_4$)-induced mouse model of liver fibrosis was used, with both prophylactic (15 mg/kg, weeks 1-6, n=12) and therapeutic (5 and 15 mg/kg, weeks 4-6, n=15/group) once daily, oral administration of **PXS-5129A** employed. BAPN (2 mg/mL in drinking water, provided *ad libitum* and changed every second day for 6 weeks, n=15) and imatinib[47] (orally dosed at 50 mg/kg, daily for weeks 1-6, n=12) were included as controls. At the end of the study 4% of the total liver area was fibrotic in the $CCl_4$-no treatment group (as quantified by both Picro Sirius Red and α-

smooth muscle actin (α-SMA) staining). No beneficial effect was observed in the Picro Sirius Red readout with the positive controls (BAPN and imatinib) (see Supplementary Figure S3), and only the lower dose of **PXS-5129A** showed a significant reduction in fibrotic area. Given that Picro Sirius Red measures total collagen content (cross-linked and soluble), it is possible that the effects of the compound are underestimated by the overwhelming quantity of soluble collagen (i.e. although the total collagen content is unchanged, the proportion of cross-linked to soluble collagen is different). To account for this possible issue, the area of fibrosis was also quantified by staining for α-smooth muscle actin (α-SMA), a marker of myofibroblast formation (Figure 6 and Supplementary Figure S4). In this readout both positive controls showed a strong anti-fibrotic effect when dosed prophylactically, suggesting that the mechanical stress on the myofibroblasts had been reduced. When dosed prophylactically **PXS-5129A** also reduced the fibrotic area, similar to the positive controls. Additionally, therapeutic dosing effected a significant decrease in fibrosis at both 5 and 15 mg/kg doses. In this study no significant effect on ALT or AST liver function markers was observed for **PXS-5120A/PXS-5129A,** nor imatinib, whereas BAPN increased ALT and AST levels (Supplementary Figure S5).

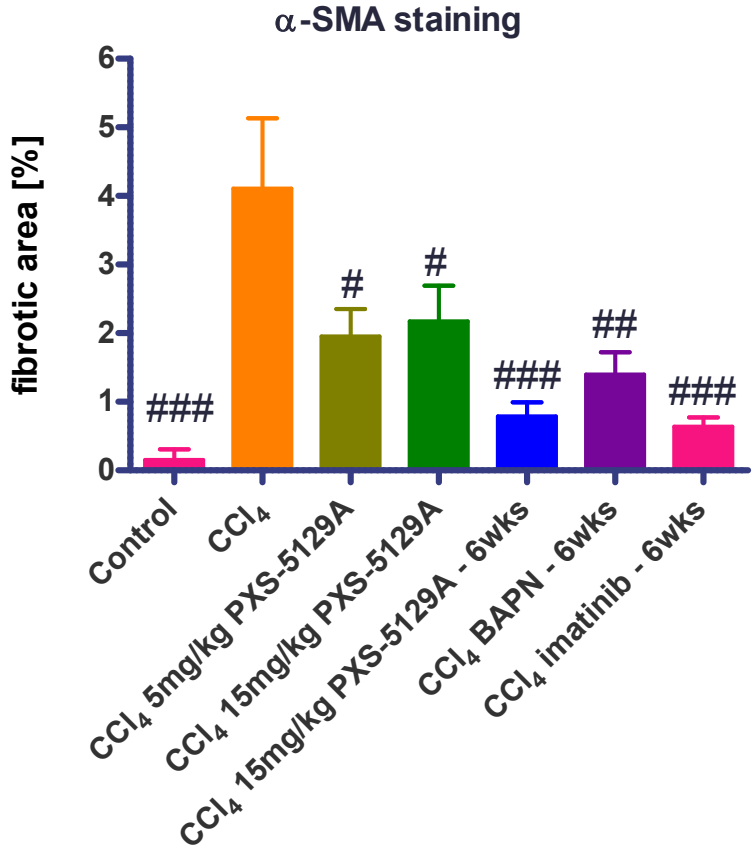


**Figure 6.** Inhibition of $CCl_4$-induced liver fibrosis by **PXS-5120A/PXS-5129A**. Quantitative measurement of fibrosis in a 6 week model of $CCl_4$-induced liver fibrosis in BALB/c mice, and the anti-fibrotic effects of **PXS-5129A**, BAPN and imatinib. The area of fibrosis was quantified by staining for α-SMA and is measured as percentage of total liver area. **PXS-5129A** reduces fibrosis when dosed both prophylactically at 15 mg/kg (6 weeks, blue bar) and therapeutically at 5 and 15 mg/kg (weeks 4-6, green bars). Results are expressed as mean ± SEM. # $p<0.05$, ## $p<0.01$ and ### $p<0.001$, *vs.* Group 2 ($CCl_4$ + vehicle); data analysis was performed by one-way ANOVA followed by Dunnett's Multiple Comparison Test.

**PXS-5120A/PXS-5129A** was also evaluated in a 28 day bleomycin-induced mouse model of lung fibrosis, using therapeutic (5 and 15 mg/kg, days 7-27, n=12/group) once daily, i.p. administration of **PXS-5129A**. Imatinib (50 mg/kg, days 7-27, n=12) was again included as a positive control.[48] An increase in fibrosis, as measured by the Ashcroft score,[49] was observed at day 28 and

therapeutic treatment with imatinib (50 mg/kg *i.p.*) afforded a small but significant reduction (Figure 7 and Supplementary Figure S6). **PXS-5129A** resulted in a dose-dependent reduction of the Ashcroft score, with the 15 mg/kg dose reaching similar effect size to the positive control imatinib. The anti-fibrotic reduction seen with imatinib in this instance is consistent with the reported effects of this drug, however the extent of the anti-fibrotic effect of imatinib is muted compared to historical data (a reduction of 50-70% is reported).[48] Given the variability of this model (potency of bleomycin used, route and frequency of administration, strain and age of mice used, etc.), this disparity is not unexpected, and the model serves to re-inforce the therapeutic potential of **PXS-5129A** in models of fibrotic disease.

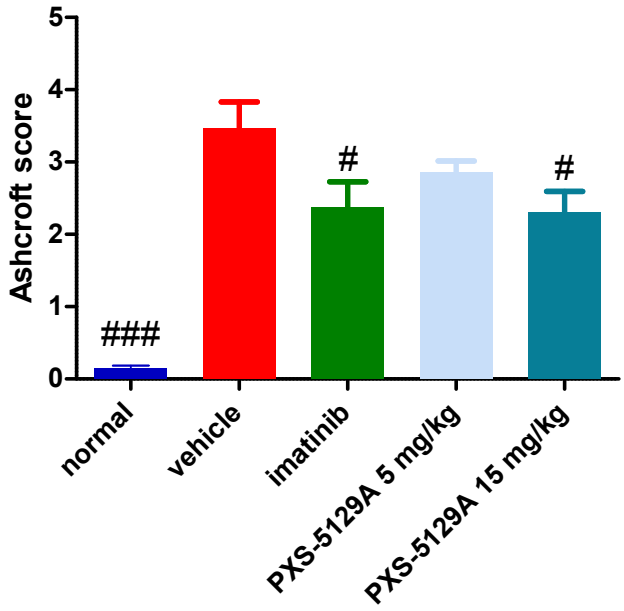


**Figure 7.** Inhibition of bleomycin-induced lung fibrosis by **PXS-5120A/PXS-5129A**. Determination of the anti-fibrotic effects of **PXS-5129A** and imatinib in a 28 day bleomycin-induced lung fibrosis in C57BL/6 mice. Analysis of the amount of fibrosis as measured by the Ashcroft score.[49] **PXS-5129A** reduces fibrosis when dosed therapeutically at 15 mg/kg (from day 7 onwards, blue bars). Results are expressed as mean ± SEM. # $p<0.05$, ## $p<0.01$ and ###

$p<0.001$, vs Group 2 (Bleo + vehicle); data analysis was performed by one-way ANOVA followed by Dunnett's Multiple Comparison Test.

## CONCLUSION

In summary, we have identified a fluoroallylamine-based lead (**4**), with inhibitory activity against SSAO, LOX and LOXL2, which has been further developed into a potent and selective inhibitor of LOXL2 (and LOXL3). Rapid exploration for additional pharmacophoric interaction points was carried out by a "Click-Chemistry" approach, resulting in the identification of a dimethyl sulfonamide as a key recognition feature required for LOXL2 potency. The potential for turnover by the related amine oxidases, SSAO and plasma amine oxidase, led us to develop a compound oxidation assay for these enzymes, which subsequently aided in the identification of the 2-methylindole core with decreased SSAO substrate activity.

Modification of the 5-position of the indole proved most effective for further optimizing LOXL2 potency and eliminating plasma amine oxidase-mediated turnover of these compounds. This afforded **PXS-5120A**, an irreversible inhibitor of LOXL2 with single-digit nanomolar potency for LOXL2, the most potent LOXL2 inhibitor reported to date. Importantly for both liver and lung diseases the additional inhibition of LOXL3 activity affords a dual inhibitor with an increased chance of reducing fibrosis in disease states.

**PXS-5120A** is selective (~300-fold) over the related LOX enzyme, which is believed to be vital for maintaining the structural integrity of the skin, heart and bone function. Equally **PXS-5120A** shows no off-target inhibition of the related amine oxidases and, importantly, is not recognized as a substrate by either SSAO or plasma amine oxidase (the *AOC4* gene product), affording a

metabolically stable compound *in vitro*, well suited for assessing the *in vivo* potential of LOXL2/LOXL3 inhibition.

As the zwitterionic nature of the compound rendered it unsuitable for direct oral administration, a pro-drug approach was employed, and the administration of **PXS-5129A** (the corresponding ethyl ester derivative of **PXS-5120A**) in two different animal models of disease successfully demonstrated the promise of selective LOXL2/3 inhibition for the treatment of liver and lung fibrosis at doses as low as 5 mg/kg.

Further progress regarding mechanism-based, orally bioavailable (without the need for a pro-drug) inhibitors of LOXL2/3 with a fast onset of inhibition and sustained target occupancy will be reported in due course.

## EXPERIMENTAL SECTION

**Chemistry General Methods.** Purity was determined by HPLC and $^{1}$H-NMR. Unless otherwise stated, the purity of final compounds was ≥95%. HPLC spectra were recorded on a Agilent LCMS 1100 instrument using reverse-phase conditions (acetonitrile/water, containing 0.1% formic acid). $^{1}$H-NMR and $^{19}$F-NMR spectra were recorded using a Bruker 300 MHz NMR spectrometer. Chemical shifts (δ) are reported as parts per million (ppm) relative to tetramethylsilane (TMS; internal standard). All commercially available solvents and reagents were used as received. Where appropriate, reactions were carried out under an argon atmosphere. Reactions were monitored by either analytical thin-layer chromatography (TLC) or by LCMS. Flash column chromatography was conducted under medium pressure either on silica (Merck silica gel 40−63 μm) or on prepacked silica gel cartridges using a flash chromatography system (CombiFlash Rf200, Teledyne Isco systems, USA), and eluents were monitored by UV light (λ = 254/280 nm). Low resolution mass spectra (MS) were obtained as electrospray – atmospheric pressure ionization (ES-API) mass spectra, which were recorded on an Agilent LCMS 1100 instrument using reverse-phase conditions

(acetonitrile/water, containing 0.1% formic acid). Melting points were obtained using a MEL-TEMP® Electrothermal melting point apparatus. All animal experiments performed were conducted in compliance with institutional guidelines and approval from local ethics committees. The general chemical methods outlined in the experimental are exemplified for the more important molecules, and may therefore be referred to before they are described in detail.

**(*S,Z*)-4-(4-Amino-2-fluorobut-2-enyloxy)-*N*-(1-phenyl ethyl)benzenesulfonamide (5).** Synthesized using chemistry outlined in reference 44.

**(*Z*)-*tert*-butyl 3-fluoro-4-hydroxybut-2-enylcarbamate (7).**

To a stirring solution of 3-amino-1,2-propanediol (20.0 g, 0.22 mol) in water (200 mL) at 0-5 °C was added di-*tert*-butyl dicarbonate (55.5 mL, 0.24 mol). After adjusting the alkalinity of the solution to pH~9 by addition of aq. NaOH (6 N), the mixture was left to stir at rt for 18 h. The reaction mixture was cooled to 0-5°C and then acidified to pH~6 before the addition of sodium metaperiodate (56.3 g, 0.26 mol). The resulting suspension was stirred at rt for 2 h. The mixture was filtered to remove all solids and the filtrate was transferred to a separatory funnel and extracted with ethyl acetate (200 mL). Sodium chloride was added to the aqueous layer until a saturated solution was obtained. The aqueous layer was then extracted further with ethyl acetate (100 mL). The combined organics were dried over $Na_2SO_4$ and then concentrated *in vacuo* to give crude *tert*-butyl 2-oxoethylcarbamate (45.7 g) as a yellow gum. The crude material was used in the subsequent step without purification.

To a stirring suspension of crude *tert*-butyl 2-oxoethylcarbamate (43.7 g, 0.22 mol) and magnesium sulfate (32.0 g) in acetonitrile (200 mL) at 0 °C under $N_2$ was added sequentially ethyl 2-fluorophosphonoacetate (55.7 mL, 0.27 mol) and 1,8-diazabicyclo[5.4.0]undec-7-ene (32.8 mL, 0.22 mol). The reaction mixture was allowed to warm to rt and stirring was continued for 3 h. After removing the solvent under reduced pressure the residue was taken up in ethyl acetate (200 mL) and then transferred to a separatory funnel. The organics were washed successively with aq. HCl (2 M; 100 mL x 2), aq. NaOH (2 M; 100 mL x 2) and brine (100 mL). After drying over $MgSO_4$, the organics were concentrated *in vacuo* to give the crude,

desired product as a mixture of *E*/*Z* isomers (2:3; 57.0 g). This crude material was progressed to the next step without purification.

To a stirring solution of crude *E*/*Z*-ethyl 4-(*tert*-butoxycarbonylamino)-2-fluorobut-2-enoate (18.0 g, 72.8 mmol) in THF (150 mL) at 0 °C under $N_2$ was added di*iso*butylaluminum hydride (1 M in toluene, 182 mL, 182 mmol) dropwise over 45 min. After complete addition, the mixture was left to stir at 0 °C for 3 h. The reaction mixture was transferred to a separatory funnel and added dropwise to a stirring mixture of ice (100 g) and aq. NaOH (2 M; 200 mL). The mixture was stirred for 2 h. The quenched reaction mixture was extracted with diethyl ether (100 mL x 2) and the combined organics were washed with brine (100 mL). After drying over $MgSO_4$ the organics were concentrated *in vacuo* to give the crude alcohol as a mixture of *E*/*Z* isomers. This mixture was purified over silica gel (135 g), eluting with 25% ethyl acetate in *n*-hexane to give (*Z*)-*tert*-butyl 3-fluoro-4-hydroxybut-2-enylcarbamate (**7**; 6.20 g, 30% over three steps) and (*E*)-*tert*-butyl 3-fluoro-4-hydroxybut-2-enylcarbamate (1.85 g, 8.9% over three steps). (*Z*)-*tert*-butyl 3-fluoro-4-hydroxybut-2-enylcarbamate (**7**): $^1$H-NMR (300 MHz; $CDCl_3$) δ ppm: 1.46 (9H, s), 3.84 (2H, dd, *J* 6.2, 6.2 Hz), 4.13 (2H, d, *J* 13.9 Hz), 4.68 (1H, br. s), 5.03 (1H, dt, *J* 36.0, 7.1 Hz). (*E*)-*tert*-butyl 3-fluoro-4-hydroxybut-2-enylcarbamate: $^1$H-NMR (200 MHz; $CDCl_3$) δ ppm: 1.43 (9H, s), 3.72 (2H, dd, *J* 7.5, 5.4 Hz), 4.25 (2H, d, *J* 21.5 Hz), 4.85 (1H, br. s), 5.18 (1H, dt, *J* 19.2, 8.5 Hz).

**(*Z*)-*tert*-butyl 4-bromo-3-fluorobut-2-enylcarbamate (8)**

To a stirring solution of (*Z*)-*tert*-butyl 3-fluoro-4-hydroxybut-2-enylcarbamate (**7**, 6.20 g, 30.2 mmol) and triethylamine (6.32 mL, 45.3 mmol) in acetone (100 mL) at 0°C was added methanesulfonyl chloride (2.81 mL, 36.3 mmol) dropwise. After complete addition the mixture was left to stir at 0 °C for 30 min. After this time, lithium bromide (13.1 g, 0.15 mol) was added portion-wise and the resulting suspension was stirred for a further 2 h. The reaction mixture was filtered to remove all solids and the filtrate was concentrated under reduced pressure. The residue was partitioned between water (50 mL) and $CH_2Cl_2$ (50 mL) and the aqueous layer was extracted with further $CH_2Cl_2$ (50 mL x 2). The combined organics were dried over $Na_2SO_4$ and concentrated *in vacuo*. The crude residue was purified over silica gel (100 g) eluting

with *n*-hexane followed by 25% ethyl acetate in *n*-hexane to afford (*Z*)-*tert*-butyl 4-bromo-3-fluorobut-2-enylcarbamate (**8**; 7.00 g, 86%) as a colorless solid. $^{1}$H-NMR (300 MHz; $CDCl_3$) δ ppm: 1.46 (9H, s), 3.85 (2H, dd, *J* 6.2, 6.2 Hz), 3.96 (2H, d, *J* 19.5 Hz), 4.66 (1H, br. s), 5.16 (1H, dt, *J* 34.0, 6.5 Hz). $^{19}$F-NMR (282 MHz; $CDCl_3$) δ ppm: -112.03.

**(*Z*)-*tert*-butyl 4-azido-3-fluorobut-2-enylcarbamate (9).** To a stirring solution of (*Z*)-*tert*-butyl 4-bromo-3-fluorobut-2-enylcarbamate (**8**) (500 mg, 1.86 mmol) in acetone (10 mL) was added sodium azide (606 mg, 9.32 mmol). The resulting suspension was stirred at rt overnight. The reaction mixture was filtered and the filter cake was washed with acetone. The filtrate was concentrated under vacuum and the residue was taken up in ethyl acetate (40 mL) and transferred to a separatory funnel. The organic layer was washed successively with water (20 mL) and brine (20 mL) then dried over $Na_2SO_4$. After removal of the solvent *in vacuo*, (*Z*)-*tert*-butyl 4-azido-3-fluorobut-2-enylcarbamate (460 mg, 100%) was obtained as a colorless oil. This material was used without purification. $^{1}$H-NMR (300 MHz; $CDCl_3$) δ ppm: 1.46 (9H, s), 3.82 (2H, d, *J* 16.4 Hz), 3.83-3.91 (2H, m), 4.66 (1H, br. s), 5.06 (1H, dt, *J* 35.1, 6.8 Hz).

**Triazole linked examples**

Compounds **10a-10k** were synthesized from commercially available phenols according to general methods A and E or F. These compounds were generated as part of a combinatorial library wherein only final compounds with a purity of ≥80% were tested in the primary screening assays. Where primary potency for LOXL2 was <100 nM (i.e. $pIC_{50} > 7.0$), compounds were either remade or re-purified to ensure that final potency was ≥95%.

**General method A**. *Preparation of N,N-dimethyl-4-prop-2-ynoxy-benzenesulfonamide*

4-hydroxy-*N,N*-dimethyl-benzenesulfonamide (150 mg, 0.75 mmol) and potassium carbonate (515 mg, 3.73 mmol) in MeCN (8 mL) was added propargyl bromide (80% in toluene) (0.25 mL, 2.24 mmol) and the resulting suspension was heated at 60 °C overnight. The reaction mixture was filtered and the filtrate was concentrated *in vacuo*. The residue was taken up in ethyl acetate (50 mL) and transferred to a separatory funnel. The organic layer was washed with water followed by brine then dried over $Na_2SO_4$ and

concentrated *in vacuo* to give N,N-dimethyl-4-prop-2-ynoxy-benzenesulfonamide (160 mg, 90%) as a yellow oil. $^1$H-NMR (300 MHz; $CDCl_3$) δ ppm: 2.60 (1H, t, *J* 2.4 Hz), 2.71 (6H, s), 4.79 (2H, d, *J* 2.4 Hz), 7.12 (2H, d, *J* 6.0 Hz), 7.75 (2H, d, *J* 6.0 Hz).

To a stirred solution of *N,N*-dimethyl-4-prop-2-ynoxy-benzenesulfonamide (66 mg, 0.28 mmol) in *t*-BuOH (1 mL) and water (1 mL) was added sodium ascorbate (1M in water) (0.1 mL, 0.1 mmol) and copper sulfate pentahydrate (1M in water) (25 μL, 0.025 mmol), followed by a solution of *tert*-butyl N-[(Z)-4-azido-3-fluoro-but-2-enyl]carbamate (**9**) (58 mg, 0.25 mmol) in t-BuOH (0.5 mL). The resulting solution was then stirred at rt overnight. The reaction mixture was partitioned between ethyl acetate and water and the organic layer was washed with brine then dried over $Na_2SO_4$ and concentrated *in vacuo*. The crude residue was purified over silica gel eluting with 50-100% EtOAc/hexane. Product *tert*-butyl N-[(Z)-4-[4-[[4-(dimethyl-sulfamoyl)phenoxy]methyl]triazol-1-yl]-3-fluoro-but-2-enyl]carbamate (84 mg, 72%) obtained as a colorless gum. $^1$H-NMR (300 MHz; $CDCl_3$) δ ppm: 2.69 (6H, d, *J* 0.9 Hz), 3.86 (2H, t, *J* 6.6 Hz), 4.76 (1H, s), 5.07 (2H, d, *J* 16.6 Hz), 5.28 (3H, m), 7.09 (2H, d, *J* 6.0 Hz), 7.74 (2H, d, *J* 6.0 Hz), 7.78 (1H, s).

**(*Z*)-3-fluoro-4-(4-(phenoxymethyl)-*1H*-1,2,3-triazol-1-yl)but-2-en-1-amine hydrochloride (10a).** Off-white solid; $^1$H-NMR (300 MHz; $d_6$-DMSO) δ ppm: 3.45-3.57 (2H, m), 5.15 (2H, s), 5.38 (2H, d, *J* 17.6 Hz), 5.43 (1H, dt, *J* 35.3, 7.3 Hz), 6.96 (1H, dd, *J* 7.3, 7.3Hz), 7.04 (2H, d, *J* 7.8 Hz), 7.31 (2H, dd, *J* 7.4, 8.6 Hz), 8.31 (1H, s). LCMS m/z 263.0 ($MH^+$). Purity 89%.

**(*Z*)-4-(4-((4-*tert*-butylphenoxy)methyl)-*1H*-1,2,3-triazol-1-yl)-3-fluorobut-2-en-1-amine hydrochloride (10b).** Brown solid; $^1$H-NMR (300 MHz; $d_6$-DMSO) δ ppm: 1.25 (9H, s), 3.45-3.57 (2H, m), 5.12 (2H, s), 5.38 (2H, d, *J* 17.5 Hz), 5.42 (1H, dt, *J* 35.3, 7.3 Hz), 6.95 (2H, d, *J* 8.9 Hz), 7.30 (2H, d, *J* 8.9 Hz), 8.27 (2H, br. s), 8.30 (1H, s). Purity 87%.

**(*Z*)-3-fluoro-4-(4-((4-(methylsulfonyl)phenoxy)methyl)-*1H*-1,2,3-triazol-1-yl)but-2-en-1-amine hydrochloride (10c).** Off-white solid; $^1$H-NMR (300 MHz; $d_6$-DMSO) δ ppm: 3.17 (3H, s), 3.46-3.57 (2H, m), 5.30 (2H, s), 5.40 (2H, d, *J* 17.6 Hz), 5.41 (1H, dt, *J* 35.2, 7.4 Hz), 7.28 (2H, d, *J* 8.9 Hz), 7.86 (2H, d, *J* 8.9 Hz), 8.19 (2H, br. s), 8.36 (1H, s).

**(*Z*)-3-fluoro-4-(4-((2-(methylsulfonyl)phenoxy)methyl)-*1*H-1,2,3-triazol-1-yl)but-2-en-1-amine hydrochloride (10d).** Off-white solid; $^1$H-NMR (300 MHz; $d_6$-DMSO) δ ppm: 3.24 (3H, s), 3.46-3.58 (2H, m), 5.32-5.51 (5H, m), 7.20 (1H, ddd, *J* 7.7, 7.7, 1.0 Hz), 7.52 (1H, d, *J* 7.8 Hz), 7.72 (1H, ddd, *J* 7.4, 8.4, 1.8 Hz), 7.82 (1H, dd, *J* 7.8, 1.8 Hz), 8.34 (1H, s). Purity 86%.

**(*Z*)-3-fluoro-4-(4-((3-(methylsulfonyl)phenoxy)methyl)-*1H*-1,2,3-triazol-1-yl)but-2-en-1-amine hydrochloride (10e).** Off-white solid; $^1$H-NMR (300 MHz; $d_6$-DMSO) δ ppm: 3.24 (3H, s), 3.47-3.58 (2H, m), 5.30 (2H, s), 5.40 (1H, dt, *J* 35.2, 7.3 Hz), 5.40 (2H, d, *J* 17.6 Hz), 7.41 (1H, ddd, *J* 8.1, 2.5, 1.1 Hz), 7.48-7.63 (3H, m), 8.12 (2H, br. s), 8.33 (1H, s). Purity 86%.

**(*Z*)-4-((1-(4-amino-2-fluorobut-2-enyl)-*1H*-1,2,3-triazol-4-yl)methoxy)-*N*,*N*-dimethylbenzamide hydrochloride (10f).** Off-white solid; $^1$H-NMR (300 MHz; $d_6$-DMSO) δ ppm: 2.95 (6H, s), 3.48-3.59 (2H, m), 5.22 (2H, s), 5.37 (1H, dt, *J* 35.0, 7.4 Hz), 5.39 (2H, d, *J* 17.3 Hz), 7.08 (2H, d, *J* 8.8 Hz), 7.39 (2H, d, *J* 8.8 Hz), 8.04 (2H, br. s), 8.30 (1H, s). LCMS m/z 334.2 ($MH^+$). Purity 84%.

**(*Z*)-4-((1-(4-amino-2-fluorobut-2-enyl)-*1H*-1,2,3-triazol-4-yl)methoxy)-*N*,*N*-dimethylbenzenesulfonamide hydrochloride (10g).** White solid; m.p. 200-202°C; $^1$H-NMR (300 MHz; $d_6$-DMSO) δ ppm: 2.57 (6H, s), 3.46-3.57 (2H, m), 5.29 (2H, s), 5.40 (2H, d, *J* 17.7 Hz), 5.43 (1H, dt, *J* 35.3, 7.3 Hz), 7.29 (2H, d, *J* 8.9 Hz), 7.70 (2H, d, *J* 8.9 Hz), 8.23 (2H, br. s), 8.37 (1H, s). $^{19}$F-NMR (282 MHz; $d_6$-DMSO) δ ppm: -109.6. LCMS m/z 370.0 ($MH^+$).

**(*Z*)-4-((1-(4-amino-2-fluorobut-2-enyl)-*1H*-1,2,3-triazol-4-yl)methoxy)-3-chloro-*N*,*N*-dimethylbenzenesulfonamide hydrochloride (10h).** White solid; m.p. 110-112°C; $^1$H-NMR (300 MHz; $d_6$-DMSO) δ ppm: 2.62 (6H, s), 3.53 (2H, m), 5.32-5.49 (5H, m), 7.64 (1H, d, *J* 8.7 Hz), 7.72-7.77 (2H, m), 8.08 (3H, br. s), 8.37 (1H, s). $^{19}$F-NMR (282 MHz; $d_6$-DMSO) δ ppm: -109.6. LCMS m/z 404.0/406.0 ($MH^+$).

**(*Z*)-4-((1-(4-amino-2-fluorobut-2-enyl)-*1H*-1,2,3-triazol-4-yl)methylamino)-*N*,*N*-dimethylbenzene sulfonamide hydrochloride (10i).** White solid; $^1$H-NMR (300 MHz; $d_6$-DMSO) δ ppm: 2.52 (6H, s), 3.45-

3.56 (2H, m), 4.40 (2H, s), 5.33 (2H, d, *J* 17.2 Hz), 5.37 (1H, dt, *J* 35.2, 7.2 Hz), 6.79 (2H, d, *J* 8.9 Hz), 7.43 (2H, d, *J* 8.8 Hz), 8.08 (1H, s), 8.16 (2H, br. s). LCMS m/z 369.0 ($MH^+$).

**(*Z*)-4-((1-(4-amino-2-fluorobut-2-en-1-yl)-*1H*-1,2,3-triazol-4-yl)methyl)-*N*,*N*-dimethylbenzenesulfonamide hydrochloride (10j).** White solid. $^1$H-NMR (300 MHz; $CD_3OD$) δ ppm: 2.68 (6H, s), 3.67 (2H, d, *J* 7.5 Hz), 4.20 (2H, s), 5.27-5.43 (3H, m), 7.53 (2H, d, *J* 8.1 Hz), 7.74 (2H, d, *J* 8.1 Hz), 7.91 (1H, br.s). LCMS m/z 354.0 ($MH^+$).

**(*Z*)-4-(1-(4-amino-2-fluorobut-2-en-1-yl)-*1H*-1,2,3-triazol-4-yl)-*N*,*N*-dimethylbenzenesulfonamide hydrochloride (10k).** Sticky white solid. $^1$H-NMR (300 MHz; $CD_3OD$) δ ppm: 2.73 (6H, s), 3.71 (2H, d, *J* 7.2 Hz), 5.33-5.49 (3H, m), 7.88 (2H, d, *J* 6.6 Hz), 8.10 (2H, d, *J* 6.6 Hz), 8.59 (1H, s). LCMS m/z 340.0 ($MH^+$).

Compounds **11a** and **11b** were synthesized starting from the commercially available *tert*-butyl 3-bromo-1H-pyrrole-1-carboxylate according to general methods B and E.

**(*Z*)-4-(1-(4-amino-2-fluorobut-2-en-1-yl)-*1H*-pyrrol-3-yl)-*N*,*N*-dimethylbenzenesulfonamide hydrochloride (11a).** Sticky white solid. $^1$H-NMR (300 MHz; $CD_3OD$) δ ppm: 2.72 (6H, s), 3.66 (2H, d, *J* 7.5 Hz), 4.81 (2H, partially obscured by $H_2O$), 5.08 (1H, dt, *J* 33.3, 7.2 Hz), 6.60 (1H, m), 6.87 (1H, m), 7.33 (1H, m), 7.69-7.76 (4H, m). LCMS m/z 338.0 ($MH^+$). Purity 91%.

**(*Z*)-3-(1-(4-amino-2-fluorobut-2-en-1-yl)-1H-pyrrol-3-yl)-*N*,*N*-dimethylbenzenesulfonamide hydrochloride (11b).** Sticky yellow solid. $^1$H-NMR (300 MHz; $CD_3OD$) δ ppm: 2.70 (6H, s), 3.66 (2H, d, *J* 7.5 Hz), 4.83 (2H, partially obscured by $H_2O$), 5.09 (1H, dt, *J* 33.0, 7.5 Hz), 6.55 (1H, m), 6.86 (1H, m), 7.29 (1H, m), 7.32-7.58 (2H, m), 7.79-7.84 (2H, m). LCMS m/z 338.0 ($MH^+$). Purity 93%.

**Indole linked examples**

Compounds **12a, b, f, g, h, i** and **j** were synthesized from commercially available indoles according to general methods B and E. Compounds **12c, d** and **e** were synthesized from commercially available indoles according to general methods B, C, D and E. Compounds **12k (PXS-5120A)** and **12l** were synthesized from commercially available indoles according to general methods B, C and F. Compound **12m** was synthesized

from commercially available 2-methyl-*1H*-indole-5-carbonitrile according to general method B followed by cycloaddition with sodium azide,[50] prior to removal of the Boc group according to general method E . Compound **12n** (des-fluoro analogue of **PXS-5120A**) was synthesized from the commercially available indole and 1-(tert-butoxycarbonylamino)-4-bromo-2-butene[51] according to general methods B, C and F. Compound **12o (PXS-5129A)** was synthesized from the commercially available indole ethyl 2-methyl-*1H*-indole-5-carboxylate according to general methods B and G.

**General method B.** *Preparation of (Z)-ethyl 1-(4-((tert-butoxycarbonyl) amino)-2-fluorobut-2-en-1-yl)-3-(3-(N,N-dimethylsulfamoyl)phenyl)-2-methyl-1H-indole-5-carboxylate.* To a stirring solution of ethyl 2-methyl-1*H*-indole-5-carboxylate (500 mg, 2.46 mmol) in $CH_2Cl_2$ (15 mL) at rt under nitrogen was added *N*-bromosuccinimide (460 mg, 2.58 mmol) in one lot. The resulting mixture was stirred at rt for 1 h then cooled to 0 °C before the addition of 4-(dimethylamino) pyridine (300 mg, 2.46 mmol) followed by a solution of di-*tert*-butyl dicarbonate (1.07 g, 4.90 mmol) in $CH_2Cl_2$ (5 mL). The mixture was allowed to slowly warm to rt over 1 h, concentrated *in vacuo* and purified over silica gel (40 g), eluting with 10% ethyl acetate in *n*-hexane, to afford 1-*tert*-butyl 5-ethyl 3-bromo-2-methyl-1*H*-indole-1,5-dicarboxylate (760 mg, 81%) as a white solid. $^1$H-NMR (300 MHz; $CDCl_3$) δ ppm: 1.45 (3H, t, *J* 7.2 Hz), 1.71 (9H, s), 2.68 (3H, s), 4.44 (2H, q, *J* 7.2 Hz), 8.02 (1H, dd, *J* 9.0, 1.8 Hz), 8.16 (1H, d, *J* 9.0 Hz), 8.19 (1H, d, *J* 1.8 Hz).

A stirred solution of 1-*tert*-butyl 5-ethyl 3-bromo-2-methyl-1H-indole-1,5-dicarboxylate (900 mg, 2.35 mmol), *N,N*-dimethyl-3-(4,4,5,5-tetramethyl-1,3,2-dioxaborolan-2-yl)benzenesulfonamide (186 mg, 0.60 mmol), aqueous potassium carbonate (2 M, 21.2 mL, 42.4 mmol) and 1,4-dioxane (9 mL) was degassed by passing a stream of nitrogen through it for 5 min. Tetrakis(triphenylphosphine)palladium(0) (272 mg, 0.24 mmol) was then added under nitrogen and the reaction mixture heated at 90 ºC for 16 h. The reaction was allowed to cool to rt, filtered through Celite and washed with ethyl acetate (20 mL). The organic layer was separated and the aqueous layer extracted with ethyl acetate (20 mL x 2). The combined organic layers were dried over $Na_2SO_4$ and concentrated *in vacuo*. The residue thus obtained was dissolved in $CH_2Cl_2$ (4 mL) and trifluoroacetic acid (4 mL) added. The mixture was stirred at rt for 1 h, then concentrated *in vacuo*. Methanol (5 mL) was added to the residue and the resultant precipitate filtered, washed with methanol (1

mL x 2) and dried under vacuum to afford ethyl 3-(3-(*N*,*N*-dimethylsulfamoyl)phenyl)-2-methyl-1*H*-indole-5-carboxylate (585 mg, 51%) as a yellow solid. $^1$H-NMR (300 MHz; $CDCl_3$) δ ppm: 1.41 (3H, t, *J* 7.1 Hz), 2.56 (3H, s), 2.84 (6H, s), 4.39 (2H, q, *J* 7.0 Hz), 7.39 (1H, d, *J* 8.5 Hz), 7.69 (1H, d, *J* 7.7 Hz), 7.75 – 7.80 (2H, m), 7.92 – 7.96 (2H, m), 8.27 (1H, br. s), 8.36 (1H, br. s).

A mixture of ethyl 3-(3-(*N*,*N*-dimethylsulfamoyl)phenyl)-2-methyl-1*H*-indole-5-carboxylate (130 mg, 0.34 mmol), cesium carbonate (132 mg, 0.4 mmol) and (*Z*)-*tert*-butyl (4-bromo-3-fluorobut-2-en-1-yl)carbamate (**8**) (99 mg, 0.37 mmol) in DMF (1.3 mL) was stirred at rt overnight. Water (13 mL) was then added, followed by brine (2.6 mL). The resultant suspension was stirred at rt for 5 min and the precipitate then filtered and dried under vacuum. The crude solid thus obtained was purified over silica gel (25 g) eluting with a mixture of *n*-hexane, $CH_2Cl_2$ and ethyl acetate in a ratio of 4:4:1, then 2:2:1 to afford (*Z*)-ethyl 1-(4-((*tert*-butoxycarbonyl)amino)-2-fluorobut-2-en-1-yl)-3-(3-(*N*,*N*-dimethylsulfamoyl)phenyl)-2-methyl-1H-indole-5-carboxylate (150 mg, 78%) as a light grey oil. $^1$H-NMR (300 MHz; $CDCl_3$) δ ppm: 1.40 (3H, t, *J* 7.1 Hz), 1.42 (9H, s), 2.51 (3H, s), 2.83 (6H, s), 3.82 (2H, apparent t, *J* 5.2 Hz), 4.38 (2H, q, *J* 7.1 Hz), 4.73 – 4.87 (1H, m), 4.86 (2H, d, *J* 9.8 Hz), 7.35 (1H, d, *J* 8.7 Hz), 7.65 – 7.79 (3H, m), 7.90 (1H, dd, *J* 1.6, 1.6 Hz), 7.97 (1H, dd, *J* 8.7, 1.6 Hz), 8.33 (1H, d, *J* 1.2 Hz).

**General procedure C.** Preparation of (Z)-1-(4-((tert-butoxycarbonyl)amino)-2-fluorobut-2-en-1-yl)-3-(3-(N,N-dimethylsulfamoyl)phenyl)-2-methyl-1H-indole-5-carboxylic acid. To a stirring solution of (Z)-ethyl 1-(4-((tert-butoxycarbonyl)amino)-2-fluorobut-2-en-1-yl)-3-(3-(N,N-dimethylsulfamoyl)phenyl)-2-methyl-1H-indole-5-carboxylate (469 mg, 0.82 mmol) in methanol (18 mL) was added aqueous KOH (10% w/v, 9 mL). The mixture was heated at 60 °C for 1 h, then cooled to rt and concentrated *in vacuo*. The residue thus obtained was taken up in water (20 mL) and the resulting solution acidified to pH 4.5 by the addition of HCl (2 M). The product was extracted with ethyl acetate (20 mL x 3) and the combined organic layers dried over $Na_2SO_4$ and concentrated *in vacuo* to afford (*Z*)-1-(4-((*tert*-butoxycarbonyl)amino)-2-fluorobut-2-en-1-yl)-3-(3-(*N*,*N*-dimethylsulfamoyl)phenyl)-2-methyl-1*H*-indole-5-carboxylic acid (390 mg, 87%) as an off-white solid. $^1$H-NMR (300 MHz; $d_6$-DMSO) δ ppm: 1.36 (9H, s), 2.52 (3H, s), 2.70 (6H, s), 3.58 (2H, br. s), 4.98 – 5.17 (1H, m), 5.15 (2H, d, *J* 14.2 Hz), 7.00 (1H, br. s), 7.68 (1H, d, *J* 8.7 Hz), 7.71 – 7.83 (5H, m), 8.18 (1H, d, *J* 1.1 Hz), 12.49 (1H, br. s).

**General method D.** *Preparation of (Z)-tert-butyl (4-(5-(dimethylcarbamoyl)-3-(3-(N,N-dimethylsulfamoyl)phenyl)-2-methyl-1H-indol-1-yl)-3-fluorobut-2-en-1-yl)carbamate.* To a stirring mixture of dimethylamine hydrochloride (10 mg, 0.12 mmol) in DMF (0.5 mL) at rt was added triethylamine (57 μL, 0.41 mmol). After 10 min (*Z*)-1-(4-((*tert*-butoxycarbonyl)amino)-2-fluorobut-2-en-1-yl)-3-(3-(*N*,*N*-dimethylsulfamoyl)phenyl)-2-methyl-1*H*-indole-5-carboxylic acid (45 mg, 0.08 mmol) was added, followed by HATU (38 mg, 0.10 mmol). The resulting mixture was stirred at rt for 2 h and then diluted with water (10 mL). The pale yellow solid thus obtained was filtered and washed with 1 M HCl (5 mL) and water (5 mL), and then dried in oven at 60 °C to afford (*Z*)-*tert*-butyl (4-(5-(dimethylcarbamoyl)-3-(3-(*N*,*N*-dimethylsulfamoyl)phenyl)-2-methyl-1*H*-indol-1-yl)-3-fluorobut-2-en-1-yl)carbamate (45 mg, 95%) as a pale yellow solid. $^1$H-NMR (300 MHz; $CDCl_3$) δ ppm: 1.43 (9H, s), 2.52 (3H, s), 2.79 (6H, s), 3.10 (6H, br. s), 3.82 – 3.86 (2H, m), 4.71 – 4.86 (1H, m), 4.84 (2H, d, *J* 9.5 Hz), 7.34 (2H, apparent d, *J* 1.1 Hz), 7.65 (1H, dd, *J* 7.6, 7.6 Hz), 7.71 – 7.77 (3H, m), 7.87 (1H, dd, *J* 1.5, 1.5 Hz).

**(*Z*)-4-(1-(4-amino-2-fluorobut-2-en-1-yl)-2-methyl-*1H*-indol-3-yl)-*N*,*N*-dimethylbenzenesulfonamide hydrochloride (12a).** Glassy solid; m.p 145-150 ˚C; $^1$H-NMR (300 MHz; $d_6$-DMSO) δ ppm: 2.55 (3H, s), 2.68 (6H, s), 3.41 -3.53 (2H, m), 5.06 (1H, dt, *J* 36.0, 7.3 Hz), 5.20 (2H, d, *J* 12.2 Hz), 7.13 (1H, dd, *J* 7.4, 7.4 Hz), 7.21 (1H, dd, *J* 7.4, 7.4 Hz), 7.61 (2H, apparent d, *J* 7.9 Hz), 7.74 (2H, d, *J* 8.4 Hz), 7.85 (2H, d, *J* 8.4 Hz), 8.04 (3H, br. s). LCMS m/z 402.2 ($MH^+$).

**(*Z*)-3-(1-(4-amino-2-fluorobut-2-en-1-yl)-2-methyl-*1H*-indol-3-yl)-*N*,*N*-dimethylbenzenesulfonamide hydrochloride (12b)** White solid; m.p 242-245 ˚C; $^1$H-NMR (300 MHz; $d_6$-DMSO) δ ppm: 2.52 (3H, s), 2.70 (6H, s), 3.47 (2H, br. d, *J* 7.1 Hz), 5.04 (1H, dt, *J* 36.0, 7.2 Hz), 51.9 (2H, d, *J* 12.3 Hz), 7.13 (1H, ddd, *J* 7.0, 7.0, 1.0 Hz), 7.21 (1H, ddd, *J* 6.9, 6.9, 1.1 Hz), 7.53 (1H, d, *J* 7.6 Hz), 7.61 (1H, d, *J* 8.0 Hz), 7.70 (1H, dd, *J* 7.2, 1.8 Hz), 7.73 – 7.76 (1H, m), 7.79 (1H, d, *J* 7.9 Hz), 7.83 (1H, dd, *J* 7.6, 1.7 Hz), 7.97 (3H, br. s). LCMS m/z 402.2 ($MH^+$).

**General method E. Preparation of (*Z*)-1-(4-amino-2-fluorobut-2-en-1-yl)-3-(3-(*N*,*N*-dimethylsulfamoyl)phenyl)-*N*,*N*,2-trimethyl-*1H*-indole-5-carboxamide hydrochloride (12c).** To a stirring solution of (*Z*)-*tert*-butyl (4-(5-(dimethylcarbamoyl)-3-(3-(*N*,*N*-dimethylsulfamoyl)phenyl)-2-methyl-1*H*-indol-1-yl)-3-fluorobut-2-en-1-yl)carbamate (45 mg, 0.08 mmol) in methanol (1 mL) was added HCl (2 M in diethyl ether, 4 mL, 8 mmol). The reaction was then stirred for 90 min at rt, then concentrated *in vacuo*. Ethyl acetate (2 mL) was added and the resulting suspension was stirred for 5 min during which time a forming a fine white solid precipitated. The white solid was collected and dried to afford (*Z*)-1-(4-amino-2-fluorobut-2-en-1-yl)-3-(3-(*N*,*N*-dimethylsulfamoyl)phenyl)-*N*,*N*,2-trimethyl-1*H*-indole-5-carboxamide hydrochloride (37 mg, 98%) as a white solid; $^1$H-NMR (300 MHz; $d_6$-DMSO) δ ppm: 2.54 (3H, s), 2.69 (6H, s), 2.97 (6H, s), 3.43 – 3.54 (2H, m), 5.09 (1H, dt, *J* 36.0, 7.5 Hz), 5.23 (2H, d, *J* 12.5 Hz), 7.28 (1H, dd, *J* 8.4, 1.4 Hz), 7.56 (1H, d, *J* 1.3 Hz), 7.66 (1H, d, *J* 8.5 Hz), 7.69 – 7.86 (4H, m), 7.98 (2H, br. s). LCMS m/z 473.2 ($MH^+$).

**(*Z*)-1-(4-amino-2-fluorobut-2-en-1-yl)-3-(3-(*N*,*N*-dimethylsulfamoyl)phenyl)-*N*,*N*,2-trimethyl-*1H*-indole-6-carboxamide hydrochloride (12d).** White solid; m.p 140-145 ˚C; $^1$H-NMR (300 MHz; $CD_3OD$) δ ppm: 2.58 (3H, s), 2.78 (6H, s), 3.12 (3H, br. s), 3.16 (3H, br. s), 3.63 (2H, br. d, *J* 7.3 Hz), 4.89 (1H, dt, *J* 34.2, 7.5 Hz), 5.18 (2H, d, *J* 9.1 Hz), 7.24 (1H, dd, *J* 8.3, 1.3 Hz), 7.59 – 7.65 (2H, m), 7.75 – 7.87 (4H m). LCMS m/z 473.2 ($MH^+$).

**(*Z*)-1-(4-amino-2-fluorobut-2-en-1-yl)-3-(3-(*N*,*N*-dimethylsulfamoyl)phenyl)-*N*,*N*,2-trimethyl-*1H*-indole-7-carboxamide hydrochloride (12e)** White solid; m.p 244-246 ˚C; $^1$H-NMR (300 MHz; $CD_3OD$) δ ppm: 2.53 (3H, s), 2.78 (6H, s), 2.94 (3H, s), 3.24 (3H, s), 3.47-3.73 (2H, m), 4.36 (1H, dt, *J* 34.2, 7.5 Hz), 4.84 (1H, m), 5.20 (1H, d, *J* 18.9 Hz), 7.14 (1H, d, *J* 7.2 Hz), 7.23 (1H, t, *J* 7.5 Hz) 7.65 (1H, d, *J* 7.8 Hz), 7.79 – 7.85 (4H, m). LCMS m/z 473.2 ($MH^+$).

**(*Z*)-3-(1-(4-amino-2-fluorobut-2-en-1-yl)-5-chloro-2-methyl-*1H*-indol-3-yl)-*N*,*N*-dimethylbenzenesulfonamide hydrochloride (12f).** White solid; m.p 214-216 ˚C; $^1$H-NMR (300 MHz; $d_6$-DMSO) δ ppm: 2.50 (3H, partially obscured by DMSO peak), 2.70 (6H, s), 3.47 (2H, s), 5.09 (1H, dt, *J* 36.0, 7.2 Hz), 5.22 (2H, d, *J* 13.5 Hz), 7.23 (1H, d, *J* 8.7 Hz), 7.47 (1H, s), 7.65 – 7.85 (5H, m). LCMS m/z 436.0/438.0 ($MH^+$).

**(*Z*)-3-(1-(4-amino-2-fluorobut-2-en-1-yl)-5-hydroxy-2-methyl-*1H*-indol-3-yl)-*N*,*N*-dimethylbenzenesulfonamide hydrochloride (12g).** White solid; decomposes at 130 ˚C; $^1$H-NMR (300 MHz; $d_6$-DMSO) δ ppm: 2.50 (3H, partially obscured by DMSO peak), 2.70 (6H, s), 3.47 (2H, s), 4.92-5.22 (3H, m), 6.69 (1H, d, *J* 8.7 Hz), 6.88 (1H, s), 7.38 (1H, d, *J* 8.7 Hz), 7.65 – 7.77 (4H, m), 8.00 (3H, br.s), 8.90 (1H, s). LCMS m/z 473.2 ($MH^+$). LCMS m/z 418.2 ($MH^+$).

**(*Z*)-3-(1-(4-amino-2-fluorobut-2-en-1-yl)-5-methoxy-2-methyl-*1H*-indol-3-yl)-*N*,*N*-dimethylbenzenesulfonamide hydrochloride (12h).** White sticky solid; $^1$H-NMR (300 MHz; $d_6$-DMSO) δ ppm: 2.50 (3H, partially obscured by DMSO peak), 2.71 (6H, s), 3.46 (2H, d, *J* 6.6 Hz), 3.73 (3H, s), 5.01 (1H, dt, *J* 36.0, 7.2 Hz), 5.10 (2H, d, *J* 12.0 Hz), 7.84 (1H, d, *J* 9.0 Hz), 7.00 (1H, s), 7.51 (1H, d, *J* 8.7 Hz), 7.68 – 7.81 (4H, m), 7.96 (3H, br.s). LCMS m/z 432.2 ($MH^+$).

**(*Z*)-3-(1-(4-amino-2-fluorobut-2-en-1-yl)-2-methyl-5-(methylsulfonamido)-*1H*-indol-3-yl)-*N*,*N*-dimethylbenzenesulfonamide hydrochloride (12i).** White solid; m.p 162-170 ˚C; $^1$H-NMR (300 MHz; $CD_3OD$) δ ppm: 2.55 (3H, s), 2.79 (6H, s), 2.89 (3H, s), 3.63 (2H, d, *J* 7.2 Hz), 4.87 (1H, partially obscured by H2O peak), 5.12 (1H, d, *J* 8.4 Hz), 7.14 (1H, d, *J* 8.7 Hz), 7.50 (2H, m) 7.75 (1H, m), 7.85 (1H, s). LCMS m/z 495.3 ($MH^+$).

**(*Z*)-3-(1-(4-amino-2-fluorobut-2-en-1-yl)-2-methyl-5-(methylsulfonyl)-*1H*-indol-3-yl)-*N*,*N*-dimethylbenzenesulfonamide hydrochloride (12j).** White solid; m.p 285-289 ˚C; $^1$H-NMR (300 MHz; $d_6$-DMSO) δ ppm: 2.57 (3H, s), 2.72 (6H, s), 3.18 (3H, s), 3.47 (2H, s), 5.09 (1H, dt, *J* 36.0, 7.2 Hz), 5.32 (2H, d, *J* 12.9 Hz), 7.73 – 7.91 (6H, m), 8.05 (3H, br.s). LCMS m/z 480.2 ($MH^+$).

**General method F. Preparation of (*Z*)-1-(4-amino-2-fluorobut-2-en-1-yl)-3-(3-(*N*,*N*-dimethylsulfamoyl)phenyl)-2-methyl-*1H*-indole-5-carboxylic acid hydrochloride (12k – PXS-5120A).** To a stirring solution of (*Z*)-1-(4-((*tert*-butoxycarbonyl)amino)-2-fluorobut-2-en-1-yl)-3-(3-(*N,N*-dimethylsulfamoyl)phenyl)-2-methyl-1H-indole-5-carboxylic acid (200 mg, 0.37 mmol) in $CH_2Cl_2$ (4 mL), was added trifluoroacetic acid (1 mL). The resulting mixture was stirred at rt for 1 h then concentrated *in vacuo*. The solid thus obtained was purified over C-18-reversed phase silica gel (40 g), eluting over a gradient of 20-50% acetonitrile in water (+ 0.1% HCl) to afford (*Z*)-1-(4-amino-2-fluorobut-2-en-1-yl)-3-(3-(N,N-dimethylsulfamoyl)phenyl)-2-methyl-1H-indole-5-carboxylic acid hydrochloride (102 mg, 58%) as an off-white solid; m.p. 253-254 ºC; $^1$H-NMR (300 MHz; $d_6$-DMSO) δ ppm: 2.55 (3H, s), 2.71 (6H, s), 3.48 (2H, br. d, *J* 7.0 Hz), 5.09 (1H, dt, *J* 35.9, 7.3 Hz), 5.26 (2H, d, *J* 12.8 Hz), 7.69 – 7.86 (6H, m), 7.94 (1H, br. s), 8.20 (1H, d, *J* 1.2 Hz), 12.58 (1H, br. s). $^{19}$F-NMR (282 MHz; $d_6$-DMSO) δ ppm: -109.2. LCMS m/z 446.3 ($MH^+$).

**(*Z*)-1-(4-amino-2-fluorobut-2-en-1-yl)-3-(3-(*N*,*N*-dimethylsulfamoyl)phenyl)-2-methyl-*1H*-indole-6-carboxylic acid hydrochloride (12l) .** White solid; m.p 255-257 ˚C; $^1$H-NMR (300 MHz; $d_6$-DMSO) δ ppm: 2.56 (3H, s), 2.70 (6H, s), 3.49 (2H, br. s), 5.02 (1H, dt, *J* 35.9, 7.3 Hz), 5.32 (2H, d, *J* 12.0 Hz), 7.58 (1H, d, *J* 8.3 Hz), 7.70 – 7.88 (5H, m), 7.94 (2H, br. s), 8.25 (1H, s), 12.67 (1H, s). LCMS m/z 446.2 ($MH^+$).

**(*Z*)-3-(1-(4-amino-2-fluorobut-2-en-1-yl)-2-methyl-5-(*1H*-tetrazol-5-yl)-*1H*-indol-3-yl)-*N*,*N*-dimethylbenzenesulfonamide hydrochloride (12m).** Off-white solid; m.p. 242-247 °C; $^1$H-NMR (300 MHz; $CD_3OD$) δ ppm: 2.60 (3H, s), 2.80 (6H, s), 3.65 (2H, d, *J* 7.5 Hz), 4.95 (1H, partially obscured by $H_2O$ peak), 5.22 (2H, d, *J* 9.6 Hz), 7.72 (1H, d, *J* 8.7 Hz), 7.81 – 7.93 (5H, m), 8.27 (1H, s). LCMS m/z 469.6 ($M^+$).

**(*E*)-1-(4-aminobut-2-en-1-yl)-3-(3-(*N*,*N*-dimethylsulfamoyl)phenyl)-2-methyl-*1H*-indole-5-carboxylic acid hydrochloride (12n).** Brown solid; m.p. 224-227 °C; $^1$H-NMR (300 MHz; $CD_3OD$) δ ppm: 2.54 (s, 3H), 2.79 (s, 6H), 3.52 (d, J = 6.8 Hz, 2H), 5.00 (dd, J = 4.4, 1.9 Hz, 2H), 5.26 (dt, J = 15.5, 6.6 Hz, 1H), 6.33 – 6.02 (m, 1H), 7.46 (d, J = 8.6 Hz, 1H), 7.95 – 7.72 (m, 5H), 8.31 (d, J = 1.6 Hz, 1H). LCMS m/z 428.2 ($M^+$).

**General method G. Preparation of (*Z*)-ethyl 1-(4-amino-2-fluorobut-2-en-1-yl)-3-(3-(*N*,*N*-dimethylsulfamoyl)phenyl)-2-methyl-*1H*-indole-5-carboxylate hydrochloride (12o – PXS-5129A).** To a stirring solution of (*Z*)-ethyl 1-(4-((*tert*-butoxycarbonyl)amino)-2-fluorobut-2-en-1-yl)-3-(3-(*N,N*-dimethylsulfamoyl)phenyl)-2-methyl-1H-indole-5-carboxylate (510 mg, 0.89 mmol) in ethanol (5 mL) was added HCl (2 M in diethyl ether, 20 mL, 40 mmol). The reaction was stirred for 5 h at rt, then concentrated *in vacuo*. Diethyl ether (25 mL) was added and the resulting suspension stirred for 5 min during which time a fine off-white solid precipitated. The solid was collected and dried to afford ethyl (Z)- 1-(4-amino-2-fluorobut-2-en-1-yl)-3-(3-(N,N-dimethylsulfamoyl)phenyl)-2-methyl-1H-indole-5-carboxylate hydrochloride (403 mg , 89%) as an off-white solid; m.p. 145-147 °C; $^1$H-NMR (300 MHz; $d_6$-DMSO) δ ppm: 1.30 (3H, t, *J* 7.1 Hz), 2.55 (3H, s), 2.73 (6H, s), 3.48 (2H, br. d, *J* 7.3 Hz), 4.28 (2H, q, *J* 7.1 Hz), 5.11 (1H, dt, *J* 33.8, 7.5 Hz), 5.27 (2H, d, *J* 8.8 Hz), 7.72 – 7.86 (6H, m), 8.02 (3H, br. s), 8.19 (1H, d, *J* 1.2 Hz). $^{19}$F-NMR (282 MHz; $d_6$-DMSO) δ ppm: -109.3 LCMS m/z 474.2 ($MH^+$).

**Enzymatic Assays.** The measurement of all of the enzymatic activities was based on the detection of hydrogen peroxide with an Amplex-Red oxidation assay,[46] miniaturized in 384 well format, with the

appropriate combination of substrate and assay buffer for each individual enzyme. After 30 minute pre-incubation of the enzyme at 37 °C with the test compound (or with different incubation times for the time-dependency assay), one volume of reaction mixture containing 120 μM Amplex Red (AR) (Life Technologies), 1.5 U/mL horseradish peroxidase (HRP) (Sigma-Aldrich) and the specific substrate was mixed to each sample. The relative fluorescence units (RFU) were then measured every 2.5 minutes for 30 minutes at 37°C, excitation 565 nm and emission 590, on a BMG Clariostar Microplate Reader. All the substrates were used at concentrations related to their Km towards the corresponding enzyme, or with a range of different concentrations for the substrate competition experiments. Lysyl oxidase assay buffer contained 1.2 M urea, 50 mM sodium borate buffer, pH 8.2 and 100 μM β-aminoproprionitrile (BAPN, Sigma-Aldrich) was used for positive control.

Recombinant human and mouse LOXL2 (R&D Systems) were challenged with 5 mM putrescine (Sigma-Aldrich) as the substrate. Recombinant rat LOXL2 was purified in house from a proprietary clone supplied by Dr. Fernando Rodríguez Pascual, University of Madrid, Spain.

Bovine LOX was extracted by adapting the methodology from Shieh *et al*.[52] from calf aorta (mixed sex): the homogenized tissue was washed extensively with phosphate-buffered saline to remove LOX inhibitors and readily soluble proteins, and then extracted in 4 M urea, 50 mM sodium borate buffer, pH 8.2. The supernatant was washed and concentrated by means of Amicon 10 kDa centrifuge filters (Millipore) in 1.2 M urea, 50 mM sodium borate buffer, pH 8.2, and in the presence of protease inhibitors, and challenged with 10 mM Putrescine (Sigma-Aldrich) as the substrate.

Human fibroblast LOX and LOXL2 were obtained from the conditioned medium IMR90 cells (ATCC CCL-186) as follows: cells were cultured in MEM, 10% FBS, supplemented with 1% penicillin/streptomycin and nonessential amino acids until 80% confluent, rinsed once with phenol red free, 0.1% FBS medium, and then fed with this medium for 48-72 hours. The medium was then collected and concentrated 40-fold by centrifugation in Millipore/Amicon filtration tubes with a 10 kDa cutoff membrane.

The separation between LOX (~30 kDa) and LOXL2 (>90 kDa) was obtained by applying a second filtration with a 50 kDa cutoff membrane, after having adjusted the buffer to 50 mM sodium borate and 6 M urea, pH 8.2, to facilitate the separation of the isozymes. After the separation, the urea concentration of the samples was diluted back to 1.2 M with 50 mM sodium borate, pH 8.2. Mouse lung fibroblast LOX was obtained in a similar fashion to human, extracting the fibroblasts from homogenized mouse lung tissue and culturing as above.

Recombinant human LOXL1 was expressed and purified from cDNA (GeneArt) and 10 mM putrescine was used as substrate. 2 mM putrescine was used as the substrate for recombinant human LOXL3 (R&D Systems) and LOXL4 (Dr. Fernando Rodríguez Pascual, university of Madrid, Spain) assays.

Recombinant human semicarbazide sensitive amine oxidase (SSAO/VAP1), diamine oxidase (DAO) and monoamine oxidases A and B (MAO-A and MAO-B) assays were performed as previously described.[53]

**Collagen oxidation.** The collagen oxidation assay was based on the release of hydrogen peroxide as previously described.[17b] In a 384 black well plate, 25 μL of collagen (rat tail, type I, Thermo Fisher, 1.5 mg/mL in 50 mM sodium borate buffer, pH 8.2) was combined with 25 μL rhLOXL2 (R&D Systems) with or without the pan-lysyl oxidase inhibitor BAPN (100 μM, Sigma-Aldrich) or **PXS-5120A**. A reaction mixture using AR (120 μM; Life Technologies) and HRP (1.5 U/mL; Sigma-Aldrich) was prepared in 50 mM sodium borate buffer. 50 μL of the reaction mixture was added into each well. The relative fluorescence units (RFU) were read every 1 minute for 3 hours at 37 °C, excitation 565 nm and emission 590 nm (Clariostar, BMG labtech). The slope per minute of the kinetic curves for each sample was calculated using MARS data analysis software (BMG labtech) in the linear phase (between the 20-40 minute time points).

**Off-target profiling. PXS-5120A** was tested at Eurofins Scientific (formerly Cerep), France at a concentration of 10 μM against a panel of 119 enzyme and receptor proteins according to standard conditions. Inhibition/reduction of radioligand binding of >50% was considered a hit. See Supplementary Information for a full readout of the targets profiled.

**Determination of Kinetic Parameters**. The kinetic parameters for **PXS-5120A** and LOXL2 were determined according to the Kitz–Wilson method as previously described for SSAO.[54,55]

**Compound oxidation assay.** This assay measures the substrate turnover of a compound relative to background (dimethyl sulfoxide only). Compound oxidation by either SSAO or AOC4 (from diluted dog serum) was measured by fluorometric assay[56] over a period of 40 minutes at 37 °C in HEPES buffer in the presence of Amplex Red (20 μM), horseradish peroxidase (4 U/ml), and the test compound (at a final concentration of 30 μM). The total formation of resorufin over time was measured using an Optima reader (BMG Labtech GmbH, Ortenburg, Germany), at 37°C. Benzylamine (at 600 μM) was used as the positive control. The relative values for Benzylamine controls were 101.9 (±5.7 SEM, n=17) for human recombinant SSAO, and 25.5 (±2.9 SEM, n=17) for dog AOC4, relative to DMSO levels. Values around 1 identify compounds that are indistinguishable from DMSO = no turnover.

**Substrate competition experiment.** The measurement of substrate competition was based on the release of hydrogen peroxide as described above for the standard assay protocol. Recombinant LOXL2 was incubated with the inhibitor and differing concentrations of the substrate (putrescine) prior to addition of the reaction mixture.

**Jump dilution experiment.** The measurement of the residence time was based on the detection of hydrogen peroxide with an Amplex-Red oxidation assay, and as described in Copeland et al.[57] in a 96 well format. The target was incubated with the test compound at 30 x $IC_{50}$ for 60 minutes at 37 °C in SnapStrip PCR vials. After the incubation, a 50-fold dilution was carried out by adding the standard assay buffer, immediately followed by a 1:2 dilution with an equal volume of reaction mixture and subjected to measurement as described in the enzymatic assay methodology. The target percentage activity was measured as a function of time after the dilution event.

**Washout experiment with plate bound LOXL2.** Flat, clear bottom, high binding 96 well plates were spotted with 30 μl of 30 nM LOXL2 in coating buffer (3.03 g/L $Na_2CO_3$, 6g/L $NaHCO_3$, pH 9.6), then

sealed and left 24 hours at 4 °C. After the wells were washed three times in TBS-T (0.05% Tween 20), 100 µL of PBS plus ions (1 mM $MgCl_2$ and 2 mM $CaCl_2$) were added to the wells and incubated for 30 minutes at 37 °C in presence of the inhibitors at a concentration of 10 x $IC_{50}$. Wells were then emptied and washed three times with PBS plus ions, before receiving 200 µL of Amplex Red/HRP reaction mix (60 µM AR, 2 U/ml HRP, 5 mM Putrescine) just before being measured as described in the enzymatic assay methodology.

**ADME assays.** Protein plasma binding, microsomal and plasma stability studies were carried out at Sundia Meditech Company (Shanghai, China). Hepatocyte stability studies were carried out at GVK Bio (Hyderabad, India).

***In vivo* studies in mice.** All animal experiments performed in the manuscript were conducted in compliance with institutional guidelines.

**Pharmacokinetic studies in mice.** Studies were performed by GVK Bio (Hyderabad, India), with local ethics approval. Male BALB/c mice were administered **PXS-5129A** by oral gavage at 20 mg/kg (n= 3). Plasma was analyzed for **PXS-5129A** and **PXS-5120A** by high-performance liquid chromatography-mass spectrometry/ mass spectrometry (LCMS/MS).

**$CCl_4$-Induced Liver Fibrosis/Cirrhosis Model.** The study was performed by PharmaLegacy (Shanghai, China) with approval from the local ethics committee. Female BALB/c mice were injected intraperitoneally with $CCl_4$ (i.p.). 1 mL/kg 25% $CCl_4$ in olive oil (100 µL for a regular mouse with body weight of 25g), twice per week for a total period of 6 weeks. Animals were sacrificed 48 hours after the last $CCl_4$ administration. Test articles were dosed as outlined in the main text, sham group n=6, vehicle group n=12. Alanine aminotransferase (ALT) and aspartate aminotransferase (AST) levels were assessed in the plasma. One lobe of the liver tissue was fixed in 10% formalin and stained for Picro Sirius Red and α-SMA. Slides were scanned using a uSCOPE-GX device with a 20X lens (Microscopes International). Images were then further expanded 20X electronically and a histomorphometric evaluation was performed to determine the area of fibrosis as a percentage of the total liver area.

**Bleomycin-Induced Lung Fibrosis Model.** The study was performed at the University of Newcastle with approval from the local ethics committee. Female 6- to 8-week old C57BL/6 mice were anesthetized with isoflurane and then administered bleomycin sulphate (BP Biomedicals, NSW, Aust.) intranasally at a dose of 0.05 U/mouse in a total volume of 50 μL PBS. Control mice received the same volume of PBS and mice were sacrificed after 28 days.[58] Test articles were dosed as outlined in the main text, sham group n= 6, vehicle group n = 12. Formalin fixed lungs sections stained with haematoxylin and eosin were assessed for fibrosis in all mice as per the scale outlined by Ashcroft *et al*.[49] The whole lung sections were imaged by Aperio CS2 scanner (Lecia Biosystems) and all pictures were visualized and analyzed using Aperio ImageScope system (Leica Biosystems). Scoring was performed on randomized and masked slides. 30 frames per slide were taken at 20x magnification by a computerized software and then assessed one by one manually. Results of the 30 pictures were then averaged and represent the value for one individual mouse lung.

ASSOCIATED CONTENT

**Supporting Information**.

The following information is available in PDF format in the supporting information file;

Collagen oxidation assay

Kitz-Wilson plot for **PXS-5120A**

Picro Sirius Red and ALT/AST readouts from $CCl_4$ liver fibrosis model

IHC staining for both models

Analytical data for key compounds

CEREP off-target screening results for **PXS-5120A (12k)**

Molecular Formula (SMILES string) of each compound along with relevant *in vitro* data (.csv file)

## AUTHOR INFORMATION

### Corresponding Authors

*Alison Findlay, email: alison.findlay@pharmaxis.com.au. Phone: +61 2 9454 7200. Fax: +61 2 9451 3622; Jonathan Foot, email: jonathan.foot@pharmaxis.com.au. Phone: +61 2 9454 7200. Fax: +61 2 9451 3622.

### Present Addresses

⊥ Andrew Jarnicki, Dept. Pharmacology and Therapeutics, University of Melbourne, Parkville, Victoria 3010, Australia. Email: andrew.jarnicki@unimelb.edu.au. Phone +61 3 8344 5746

### Funding Sources

All studies were fully funded by Pharmaxis Ltd., 20 Rodborough Road, Frenchs Forest, NSW 2086, Australia. P.M.H was additionally supported by a fellowship from the National Health and Medical Research Council (NHMRC) of Australia (1079187).

## ACKNOWLEDGMENTS

The authors would like to thank Dr. Fernando Rodríguez Pascual, University of Madrid, Spain, for kindly providing recombinant rat LOXL2 clones and recombinant human LOXL4 protein.

## ABBREVIATIONS

ALT, alanine aminotransferase; AOC, amine oxidase, copper containing; AST, aspartate aminotransferase; BAPN, β-aminopropionitrile; DAO, diamine oxidase; DIPEA, diisopropyl ethylamine; ECM, extracellular matrix; EMT, epithelial-mesenchymal transition; FAD, flavin adenine dinucleotide; HATU, hexafluorophosphate azabenzotriazole tetramethyl uronium; HIF-1α, hypoxia-inducible factor-1α; HLM, human liver microsomes; HPC, hepatic progenitor cell; HRP, horseradish peroxidase; IPF, idiopathic pulmonary fibrosis; KDM1A, lysine (K)-specific demethylase 1A; LOX, lysyl oxidase; LOXL, lysyl oxidase-like; LOXL2, lysyl oxidase-like 2; LOXL3, lysyl oxidase-like 3; LSD1, Lysine-specific histone demethylase 1A; LTQ, lysine tyrosylquinone; MAO, monoamine oxidase; NASH, non-alcoholic steatohepatitis; PAO, polyamine oxidase; SRCR, scavenger receptor cysteine-rich; α-SMA, α-smooth muscle actin; SSAO, semicarbazide-sensitive amine oxidase; TGFβ, transforming growth factor beta; TPQ, topaquinone.

REFERENCES

(1) Dostert, P.L.; Benedetti, M. S.; Tipton, K.F. Interactions of monoamine oxidase with substrates and inhibitors. *Med. Res. Rev.* **1989**, *9*, 45-89.

(2) Holtta, E. Oxidation of spermidine and spermine in rat liver: purification and properties of polyamine oxidase. *Biochemistry* **1977**, *16*, 91–100.

(3) Shi, Y.; Lan, F.; Matson, C.; Mulligan, P.; Whetstine, J. R.; Cole, P. A.; Casero, R. A.; Shi, Y. Histone demethylation mediated by the nuclear amine oxidase homolog LSD1. *Cell* **2004**, *119*, 941-953.

(4) Finney, J.; Moon, H.J.; Ronnebaum, T.; Lantz, M.; Mure, M. Human copper-dependent amine oxidases. *Arch. Biochem. Biophys.* **2014**, *546*, 19-32.

(5) Bieganski, T.; Kusche, J.; Lorenz, W.; Hesterberg, R.; Stahlknecht, C. D.; Feussner, K. D. Distribution and properties of human intestinal diamine oxidase and its relevance for the histamine catabolism. *Biochim. Biophys. Acta* **1983**, *756*, 196–203.

(6) Kaitaniemi, S.; Elovaara, H.; Grön, K.; Kidron, H.; Liukkonen, J.; Salminen, T.; Salmi, M.; Jalkanen, S.; Elima, K. The unique substrate specificity of human AOC2, a semicarbazide-sensitive amine oxidase. *Cell. Mol. Life Sci.* **2009**, *66*, 2743-2757.

(7) (a) Salmi, M.; Jalkanen, S. Vascular Adhesion Protein-1: A cell surface amine oxidase in translation. *Antioxid. Redox Signal.* **2019**, *30*, 314-332. (b) Jarnicki, A.G., Schilter, H.C., Liu, G., Wheeldon, K., Esslifie, A.T., Foot, J.S., Yow, T.T., Jarolimek, W., Hansbro, P.M. The inhibitor of semicarbazide-sensitive amine oxidase, PXS-4728A, ameliorates key features of chronic obstructive pulmonary disease in a mouse model. *Br. J. Pharmacol.* **2016**, *173*, 3161-3175.

(8) Schwelberger, H.G. The origin of mammalian plasma amine oxidases. *J. Neural Transm.* **2007**, *114*, 757-762.

(9) Barker, H.E., Cox, T.R., and Erler, J.T. The rationale for targeting the LOX family in cancer. *Nat. Rev. Cancer* **2013**, *12*, 540-552.

(10) Grau-Bové, X., Ruiz-Trillo, I., Rodriguez-Pascual, F. Origin and evolution of lysyl oxidases. *Sci. Rep.* **2015**, *5*, 10568.

(11) (a) Ricard-Blum, S., Ville, G. Collagen cross-linking. *Int. J. Biochem.* **1989** *21*, 1185-1189. (b) Yamauchi, M.; Sricholpech, M. Lysine post-translational modifications of collagen. *Essays Biochem.* **2012**, *52*, 113−133.

(12) (b) Startcher, B. C. Elastin and the lung. *Thorax* **1986**, *41*, 577-585. (b) Herchenhan, A., Uhlenbrock, F., Eliasson, P., Weis, M., Eyre, D., Kadler, K. E., Magnusson, S. P., and Kjaer, M.

Lysyl oxidase activity is required for ordered collagen fibrillogenesis by tendon cells. *J. Biol. Chem.* **2015** *290*, 16440-16450.

(13) (a) He Y., Jin L., Wang J., Yan Z., Chem T., Zhao Y. Mechanisms of fibrosis in acute liver failure. *Liver Int*. **2015** *35*, 1877-1885. (b) Boor, P., Sebekova, K., Ostendorf, T., Floege, J. Treatment targets in renal fibrosis. *Nephrol. Dial. Transplant.* **2007,** *22*, 3391-3407.

(14) Pischon, N., Mäki, J. M., Weisshaupt, P., Heng, N., Palamakumbura, A. H., N'Guessan, P., Ding, A., Radlanski, R., Renz, H., Bronckers, T. A., Myllyharju, J., Kielbassa, A. M., Kleber, B. M., Bernimoulin, J. P., Trackman, P. C. Lysyl oxidase (lox) gene deficiency affects osteoblastic phenotype. *Calcif Tissue Int.,* **2009,** *85,*119-126.

(15) Mäki, J.M., Sormunen, R., Lippo, S., Kaarteenaho-Wiik, R., Soininen, R., Myllyharju, J. Lysyl oxidase is essential for normal development and function of the respiratory system and for the integrity of elastic and collagen fibers in various tissues. *Am. J. Pathol.* **2005**, *167*, 927–936.

(16) Rodríguez, C., Martínez-González, J., Raposo, B., Alcudia, J. F., Guadall, A. and Badimon, L. Regulation of lysyl oxidase in vascular cells: lysyl oxidase as a new player in cardiovascular diseases, *Cardiovascular Research*, **2008**, *79*, 7–13.

(17) (a) Barry-Hamilton, V., Spangler, R., Marshall, D., McCauley, S., Rodriguez, H. M., Oyasu, M., Mikels, A., Vaysberg, M., Ghermazien, H., Wai, C., Garcia, C. A., Velayo, A. C., Jorgensen, B., Biermann, D., Tsai, D., Green, J., Zaffryar-Eilot, S., Holzer, A., Ogg, S., Thai, D., Neufeld, G., Van Vlasselaer, P., and Smith, V. Allosteric inhibition of lysyl oxidase-like-2 impedes the development of a pathologic microenvironment. *Nat. Med.* **2010**, *16*, 1009-1017. (b) Schilter, H., Findlay, A. D., Perryman, L., Yow, T. T., Moses, J., Zahoor, A., Turner, C.I., Deodhar, M., Foot, J.S., Zhou, W., Greco, A., Joshi, A., Rayner, B., Townsend, S., Buson, A., Jarolimek, W.

The lysyl oxidase like 2/3 enzymatic inhibitor, PXS-5153A, reduces crosslinks and ameliorates fibrosis. *J. Cell. Mol. Med.* **2019**, *23*, 1759-1770.

(18) (a) Vadasz, Z., Kessler, O., Akiri, G., Gengrinovitch, S., Kagan, H. M., Baruch, Y. Izhak, O. B., Neufeld, G. Abnormal deposition of collagen around hepatocytes in Wilson's disease is associated with hepatocyte specific expression of lysyl oxidase and lysyl oxidase like protein-2. *J. Hepatol.* **2005**, *43*, 499–507; (b) Dongiovanni, P., Meroni, M., Baselli, G. A., Bassani, G. A., Rametta, R., Pietrelli, A., Maggioni, M., Facciotti, F.,Trunzo, V., Badiali, S., Fargion, S., Gatti, S., Valenti, L. Insulin resistance promotes lysyl oxidase like 2 induction and fibrosis accumulation in non-alcoholic fatty liver disease. *Clin. Sci.* **2017**, *131*, 1301–1315.

(19) Chien, J. W., Richards, T. J., Gibson, K. F., Zhang, Y., Lindell, K. O., Shao, L., Lyman, S. K., Adamkewicz, J. I., Smith, V., Kaminski, N., O'Riordan, T. Serum lysyl oxidase-like 2 levels and idiopathic pulmonary fibrosis disease progression. *Eur. Resp. J.* **2014,** *43,* 1430-1438.

(20) Cheng, Y., Wang, X., Zhang, X., Zhang, N., Zhang, X. Comparison of Loxl-2 expression between active systematic scleroderma and active mixed connective tissue disease *J. China Medical University* **2016**, *45*, 414-416.

(21) (a) Janyasupab. M., Lee, Y. H., Zhang, Y., Liu, C. W., Cai, J., Popa, A., Samia, A., C., Wang K. W., Xu, J., Hu, C. C., Wendt, M. K., Schiemann, B.J., Thompson, C. L., Yen, Y., Schiemann, W. P., Liu, C. C. Detection of lysyl oxidase-like 2 (LOXL2), a biomarker of metastasis from breast cancers using human blood samples. *Recent Pat Biomark.* **2015**, *5*, 93-100. (b) Torres, S., Garcia-Palmero, I., Herrera, M., Bartolomé, R. A., Peña, C., Fernandez-Aceñero, M. J., Padilla, G., Peláez-García, A., Lopez-Lucendo, M., Rodriguez-Merlo, R., García de Herreros, A., Bonilla, F., Casal, J. I. LOXL2 is highly expressed in cancer-associated fibroblasts and associates to poor colon cancer survival. *Clin. Cancer Res.* **2015**, *21*, 4892-4902.

(22) Pollheimer, M. J., Racedo, S., Mikels-Vigdal, A., Marshall, D., Bowlus, C., Lackner, C., Madl, T., Karlsen, T. H., Hov, J. R., Lyman, S. K., Adamkewicz, J., Smith, V., Moreau, E., Zollner, G., Eide, T. J., Stojakovic, T., Scharnagl, H., Gruber, H. J., Stauber, R. E., Trauner, M., Fickert, P. Lysyl oxidase-like protein 2 (LOXL2) modulates barrier function in cholangiocytes in cholestasis. *J. Hepatol*. **2018**, *69*, 368-377.

(23) Ikenaga, N., Peng, Z.W., Vaid, K.A., Liu, S.B., Yoshida, S., Sverdlov, D.Y., Mikels-Vigdal, A., Smith, V., Schuppan, D., Popov, Y.V. Selective targeting of lysyl oxidase-like 2 (LOXL2) suppresses hepatic fibrosis progression and accelerates its reversal. *Gut* **2017**, *66*, 1697-1708.

(24) Rodriguez, H. M., Vaysberg, M., Mikels, A., McCauley, S., Velayo, A.C., Garcia, C., Smith, V. Modulation of lysyl oxidase-like 2 enzymatic activity by an allosteric antibody inhibitor. *J. Biol. Chem.* **2010**, *285*, 20964-20974.

(25) Puente, A., Fortea, J. I., Cabezas, J., Arias Loste, M. T., Iruzubieta, P., Llerena, S., Huelin, P., Fábrega, E., Crespo, J. LOXL2-A new target in antifibrogenic therapy? *Int. J. Mol. Sci*. **2019**, *20*, 1634.

(26) Mesarwi, O. A., Shin, M. K., Drager, L. F., Bevans-Fonti, S., Jun, J.C., Putcha, N., Torbenson, M. S., Pedrosa, R. P., Lorenzi-Filho, G., Steele, K. E., Schweitzer, M. A., Magnuson, T. H., Lidor, A. O., Schwartz, A. R., Polotsky, V. Y. Lysyl oxidase as a serum biomarker of liver fibrosis in patients with severe obesity and obstructive sleep apnea. *Sleep* **2015**, *38*, 1583-1591.

(27) (a) Aumiller, V., Strobel, B., Romeike, M., Schuler, M., Stierstorfer, B. E., and Kreuz, S. Comparative analysis of lysyl oxidase (like) family members in pulmonary fibrosis. *Sci. Rep.* **2017**, *7*, 149; (b) Chen, L., Li, S., Li, W. LOX/LOXL in pulmonary fibrosis: potential therapeutic targets. *J. Drug Target* **2018**, *20*, 1-7.

(28) (a) Kamikawaji, K., Seki, N., Watanabe, M., Mataki, H., Kumamoto, T., Takagi, K., Mizuno, K., Inoue, H. Regulation of LOXL2 and SERPINH1 by antitumor microRNA-29a in lung cancer with idiopathic pulmonary fibrosis. *J. Hum. Genet.* **2016**, *61*, 985-993; (b) Leeming, D. J., Willumsen, N., Sand, J. M. B., Holm Nielsen S., Dasgupta, B., Brodmerkel, C., Curran, M., Bager, C. L., Karsdal, M. A. A serological marker of the N-terminal neoepitope generated during LOXL2 maturation is elevated in patients with cancer or idiopathic pulmonary fibrosis. *Biochem. Biophys. Rep.* **2018**, *17*, 38-43.

(29) Wei, Y., Kim, T. J., Peng, D. H., Duan, D., Gibbons, D. L., Yamauchi, M., Jackson, J. R., Le Saux, C. J., Calhoun, C., Peters, J., Derynck, R., Backes, B. J., Chapman, H. A. Fibroblast-specific inhibition of TGF-β1 signaling attenuates lung and tumor fibrosis. *J. Clin. Invest.* **2017**, 127, 3675-3688; (b) Wen, X., Liu, Y., Bai, Y., Li, M., Fu, Q., Zheng, Y. LOXL2, a copper-dependent monoamine oxidase, activates lung fibroblasts through the TGF-β/Smad pathway. *Int. J. Mol. Med.* **2018**, *42*, 3530-3541.

(30) Raghu, G.; Brown, K. K.; Collard, H. R.; Cottin, V.; Gibson, K. F.; Kaner, R. J.; Lederer, D. J.; Martinez, F. J.; Noble, P. W.; Song, J. W.; Wells, A. U.; Whelan, T. P. M.; Wuyts, W.; Moreau, E.; Patterson, S. D.; Smith, V.; Bayly, S.; Chien, J. W.; Gong, Q.; Zhang, J. J.; O'Riordan, T. G. Efficacy of simtuzumab versus placebo in patients with idiopathic pulmonary fibrosis: a randomized, double-blind, controlled, phase 2 trial. *Lancet Respir. Med.* **2017**, *5*, 22−32.

(31) Meissner, E. G.; McLaughlin, M.; Matthews, L.; Gharib, A. M.; Wood, B. J.; Levy, E.; Sinkus, R.; Virtaneva, K.; Sturdevant, D.; Martens, C.; Porcella, S. F.; Goodman, Z. D.; Kanwar, B.; Myers, R.; Subramanian, M.; Hadigan, C.; Masur, H.; Kleiner, D. E.; Heller, T.; Kottilil, S.; Kovacs, J. A.; Morse, C. G. Simtuzumab treatment of advanced liver fibrosis in HIV and HCV-infected adults: Results of a 6- month open-label safety trial. *Liver Int.* **2016**, *36*, 1783−1792.

(32) Tang, S. S.; Trackman, P. C.; Kagan, H. M. Reaction of aortic lysyl oxidase with β-aminopropionitrile. *J. Biol. Chem.* **1983**, *258*, 4331−4338.

(33) (a) Tang, H., Leung, L., Saturno, G., Viros, A., Smith, D., Di Leva, G., Morrison, E., Niculescu-Duvaz, D., Lopes, F., Johnson, L., Dhomen, N., Springer, C., Marais, R. Lysyl oxidase drives tumour progression by trapping EGF receptors at the cell surface. *Nat. Commun.* **2017**, 1*8*, 14909. (b) Springer, C., Marais, R., Niculescu-Duvaz, D., Leung, L., Smithen, D., Callens, C., Tang, H. Methylamine Derivatives as Lysyl Oxidase Inhibitors for the Treatment of Cancer, WO 2017/141049 Al. (c) Leung, L., Niculescu-Duvaz, D., Smithen, D., Lopes, F., Callens, C., McLeary, R., Saturno, G., Davies, L., Aljarah, M., Brown, M., Johnson, L., Zambon, A., Chambers, T., Ménard, D., Bayliss, N., Knight, R., Fish, L., Lawrence, R., Challinor, M., Tang, H., Marais, R., Springer, C. Anti-metastatic inhibitors of lysyl oxidase (LOX): Design and structure-activity relationships. *J. Med. Chem.* **2019**, *62*, 5863-5884.

(34) Rowbottom M. W., Bain, G., Calderon, I., Lasof, T., Lonergan, D., Lai, A., Huang, F., Darlington, J., Prodanovich, P., Santini, A. M., King, C. D., Goulet, L., Shannon, K. E., Ma, G.L., Nguyen, K., MacKenna, D. A., Evans, J.F., Hutchinson, J. H. Identification of 4-(aminomethyl)-6-(trifluoromethyl)-2-(phenoxy)pyridine derivatives as potent, selective, and orally efficacious inhibitors of the copper-dependent amine oxidase, lysyl oxidase-like 2 (LOXL2). *J. Med. Chem.* **2017,** *60*, 4403-4423.

(35) Single and Multiple Dose Safety, Tolerability, PK and Food Effect Study Of PAT‑1251 in Healthy Adult Subjects, NCT02852551, Completed November 2016

(36) Rowbottom M. W., Hutchinson, J. H., Evans, J. F., Bain, G. Chemical Probes of Lysyl Oxidase-Like 2 and Uses Thereof, WO 2018/048928 A1

(37) Stangenberg, S., Saad, S., Schilter, H. C., Zaky, A., Gill, A., Pollock, C. A., Wong, M. G. Lysyl oxidase-like 2 inhibition ameliorates glomerulosclerosis and albuminuria in diabetic nephropathy. *Sci. Rep.* **2018**, *8*, 9423.

(38) Yu, P. H., Zuo, D. M. Inhibition of a type B monoamine oxidase inhibitor, (E)-2-(4-fluorophenethyl)-3-fluoroallylamine (MDL-72974A), on semicarbazide-sensitive amine oxidases isolated from vascular tissues and sera of different species. *Biochem Pharmacol.* **1992**, *43,* 307-312.

(39) Foot, J. S., Deodhar, M., Turner, C. I., Yin, P., van Dam, E. M., Silva, D. G., Olivieri, A., Holt, A., McDonald I. A. The discovery and development of selective 3-fluoro-4-aryloxyallylamine inhibitors of the amine oxidase activity of semicarbazide-sensitive amine oxidase/vascular adhesion protein-1 (SSAO/VAP-1). *Bioorg. Med. Chem. Lett.* **2012**, *22*, 3935–3940.

(40) O'Rourke, A. M., Wang, E. Y., Miller, A., Podar, E. M., Scheyhing, K., Huang, L., Kessler, C., Gao, H., Ton-Nu, H. T., Macdonald, M. T., Jones, D. S., Linnik, M. D. Anti-inflammatory effects of LJP 1586 [Z-3-fluoro-2-(4-methoxybenzyl)allylamine hydrochloride], an amine-based inhibitor of semicarbazide-sensitive amine oxidase activity. *J. Pharmacol. Exp. Ther.* **2008**, *324*, 867–875.

(41) Foot, J. S., Yow, T. T., Schilter, H., Buson, A., Deodhar, M., Findlay, A. D., Guo, L., McDonald I. A., Turner, C. I., Zhou, W., Jarolimek, W. PXS-4681A, a potent and selective mechanism-based inhibitor of SSAO/VAP-1 with anti-inflammatory effects in vivo. *J. Pharmacol. Exp. Ther.* **2013**, *347*, 365–374.

(42) A similar mechanism has been reported for the related vinyl fluoride, mofegiline; Milczek, E. M., Bonivento, D., Binda, C., Mattevi, A., McDonald, I. A., Edmondson, D. E., Structural and

mechanistic studies of mofegiline inhibition of recombinant human monoamine oxidase B. *J. Med. Chem.* **2008**, *51,* 8019-8026.

(43) A crystal structure of LOXL2 in a precursor state, with the copper atom missing, was published recently. Given the conformational changes needed to form the active LTQ cofactor, this structure is likely unsuitable for future structure based design efforts. Zhang, X., Wang, Q., Wu, J., Wang, J., Shi, Y., Liu, M. Crystal structure of human lysyl oxidase-like 2 (hLOXL2) in a precursor state *Proc. Natl. Acad. Sci. USA* **2018**, *115*, 3828–3833.

(44) McDonald I. A., Turner, C. I., Deodhar, M., Foot, J. S. Haloallylamine Inhibitors of SSAO/VAP-1 and Uses Therefor, WO 2009/066152 A2

(45) Rostovtsev, V. V., Green, L. G., Fokin, V. V., Sharpless, K. B., A stepwise huisgen cycloaddition process: copper(i)-catalyzed regioselective ligation of azides and terminal alkynes *Angew. Chem. Int. Ed.* **2002**, *41*, 2596-2599.

(46) Zhou, M., Diwu, Z., Panchuk-Voloshina, N., Haugland, R. P. A stable non-fluorescent derivative of resorufin for the fluorometric determination of trace hydrogen peroxide: applications in detecting the activity of phagocyte NADPH oxidase and other oxidases. *Anal. Biochem*. **1997**, *253*, 162–168.

(47) Kuo, W. L., Yu, M. C., Lee, J. F., Tsai, C. N., Chen, T. C., Chen, M. F. Imatinib mesylate improves liver regeneration and attenuates liver fibrogenesis in $CCl_4$-treated mice. *J. Gastrointest. Surg.* **2012**, *16,* 361-369.

(48) Aono, Y., Nishioka,, Y., Inayama, M., Ugai, M., Kishi, J., Uehara, H., Izumi, K., Sone, S. Imatinib as a novel antifibrotic agent in bleomycin-induced pulmonary fibrosis in mice. *Am. J. Respir. Crit. Care Med.* **2005**, *171*, 1279-1285.

(49) Ashcroft, T., Simpson, J. M., and Timbrell, V. Simple method of estimating severity of pulmonary fibrosis on a numerical scale. *J. Clin. Path.* **1988**, *41*, 467–470.

(50) Balle, T., Perregaard, J., Ramirez, M. T., Larsen, A. K., Søby, K. K., Liljefors, T., Andersen, K. Synthesis and structure-affinity relationship investigations of 5-heteroaryl-substituted analogues of the antipsychotic sertindole. A new class of highly selective α-1 adrenoceptor antagonists. *J. Med. Chem.* **2003**, *46*, 265-283.

(51) de Bruin, G., van Rooden, E. J., Ward, D., Wesseling, C., van den Nieuwendijk, A. M. C. H., van Boeckel, C. A. A., Driessen, C., Kisselev, A. F., Florea, B. I., van der Stelt, M., Overkleeft, H. S. Asymmetric synthesis of lysine analogues with reduced basicity, and their incorporation into proteasome inhibitors. *Eur. J. Org. Chem.* **2017**, *39*, 5921–5934.

(52) Shieh, J. J., Tamaye, R, Yasunobu, K. T. A purification procedure for the isolation of homogeneous preparations of bovine aorta amine oxidase and a study of its lysyl oxidase activity. *Biochim Biophys Acta.* **1975,** *377*, 229-238.

(53) Schilter, H. C., Collison, A., Russo, R. C., Foot, J. S., Yow, T. T., Vieira, A. T., Tavares, L. D., Mattes, J., Teixeira, M. M., Jarolimek, W. Effects of an anti-inflammatory VAP-1/SSAO inhibitor, PXS-4728A, on pulmonary neutrophil migration. *Respir. Res.* **2015**, *16*, 42-49.

(54) Kitz, R. and Wilson, I. B. Esters of methanesulfonic acid as irreversible inhibitors of acetylcholinesterase. *J. Biol. Chem.* **1962**, *237*, 3245–3249.

(55) Holt, A., Smith, D. J., Cendron, L., Zanotti, G., Rigo, A., Di Paolo, M. L. Multiple binding sites for substrates and modulators of semicarbazide-sensitive amine oxidases: kinetic consequences. *Mol. Pharmacol.* **2008**, *73*, 525–538.

(56) Holt, A. and Palcic, M. M. A peroxidase-coupled continuous absorbance plate reader assay for flavin monoamine oxidases, copper-containing amine oxidases and related enzymes. *Nat. Protoc*. **2006**, *1*, 2498–2505.

(57) Copeland, R. A., Basavapathruni, A., Moyer, M., Scott, M. P. Impact of enzyme concentration and residence time on apparent activity recovery in jump dilution analysis. *Anal. Biochem*. **2011**, *416*, 206-210.

(58) O'Donoghue, R. J. J., Knight, D. A., Richards, C. D., Prêle, C. M., Lau, H. L., Jarnicki, A. G., Jones, J., Bozinovski, S., Vlahos, R., Thiem, S., McKenzie, B. S., Wang, B., Stumbles, P., Laurent, G.J., McAnulty, R.J., Rose-John, S., Zhu, H. J., Anderson, G. P., Ernst, M. R., Mutsaers, S. E. Genetic partitioning of interleukin-6 signalling in mice dissociates Stat3 from Smad3-mediated lung fibrosis. *EMBO Mol. Med.* **2012**, *4*, 939–951.

## Table of Contents Graphic